Journal of Thermal Analysis and Calorimetry
https://doi.org/10.1007/s10973-022-11606-y

A review on laminar-to-turbulent transition of nanofluid flows

Abdussamet Subasi[1] · Mehmed Rafet Ozdemir[2] · Patrice Estellé[3]

Received: 22 April 2022 / Accepted: 1 September 2022

Abstract
Nanofluids have emerged as powerful instruments in heat transfer applications due to their improved thermophysical properties. Additionally, many heat transfer equipments are started to be operated within the range of transitional flow regions in the advances in thermal management enhancement techniques. However, up to date, the friction factor and heat transfer coefficient features of nanofluids within the transitional flow regions and the effect of nanoparticle addition into the base fluid on the laminar-to-turbulent transition characteristics are still not understood clearly with contradictory published results. At this point, this paper comprehensively reviews the studies dealing with the nanofluid flow within the transitional flow regions for internal flow applications. After the presentation of applications of nanofluid flow in the transitional flow regions, the nanofluid properties such as nanoparticle type and concentration and base fluid type in the reviewed studies are given in detail. The pressure drop and heat transfer features of nanofluid flow within the transitional flow regions are distinctly identified and discussed for internal flows. The effect of the nanoparticle addition into the liquid on the transition onset is discussed with results from different research groups. A complete evaluation, challenges and further studies are proposed based on available results in the literature.

Keywords Nanofluid · Laminar-to-turbulent transition · Convective heat transfer · Pressure drop

Introduction

There is a continuous increase in the world's energy consumption due to several factors such as the rapid development of technology, the increasing population of the world and industrialization. The rapid depletion of limited fossil energy resources, which respond to a great share of the energy demand of the world, necessitates production, transmission, distribution and use of energy in an efficient and economical method. For this reason, heat, which is an energy form, must also be transferred efficiently between the mediums at different temperatures as well as produced and used effectively.

The heat transfer enhancement is a commonly encountered engineering problem in many industrial applications such as cooling of nuclear reactors, gas turbines, heat pipes, heat exchangers, air-conditioning and cooling of electronic devices [1, 2, 3]. The literature on heat transfer enhancement methods states classification as passive, active and hybrid. When it is necessary to use an additional energy input it is called an active technique, whereas an additional energy input is not required for passive techniques. Examples of passive thermal management augmentation techniques can be listed as rough surfaces, extended surfaces, swirl flow devices, treated surfaces and additives. Electrostatic field injection, surface vibration and suction can be classified as active thermal management augmentation techniques. Hybrid techniques combine active and passive methods cooperatively and reveal higher heat transfer augmentation performance in comparison with using either passive or active methods independently. Although there is no need for additional power input for passive methods and the devices used are uncomplicated and cost economic, they have two major drawbacks: firstly, they cannot be optimized according

✉ Abdussamet Subasi
subasiab@itu.edu.tr

Mehmed Rafet Ozdemir
mehmet.ozdemir@marmara.edu.tr

Patrice Estellé
patrice.estelle@univ-rennes1.fr

[1] Department of Mechanical Engineering, Istanbul Technical University (ITU), 34437 Istanbul, Turkey

[2] Faculty of Engineering, Department of Mechanical Engineering, Marmara University, 34722 Istanbul, Turkey

[3] LGCGM, Université Rennes 1, 35000 Rennes, France

Published online: 01 November 2022

to multiple situations; secondly, they create extra pumping power due to enhanced pressure drop. Instead, active and hybrid heat transfer enhancement methods require expensive and complex structures [1, 4, 5, 6, 7, 8, 9]. Even if the boiling heat transfer mechanism is regarded as a promising solution due to high heat flux dissipation with less pressure drop, the underlying physical phenomena are still not clearly understood owing to the complicated characteristics of flow physics [10, 11].

Adding particles with nanometer dimensions into the fluid as ethylene glycol, water and oil is named nanofluid by Choi and Eastman [12] in 1995. Thereafter, nanofluids have received great attention by engineers and scientists being a passive heat transfer enhancement method since the second half of the twentieth century. Nanofluids have been appraised as promising heat transfer fluid since they have enhanced thermophysical characteristics compared to traditional base fluids [13, 14, 15]. Figure 1 shows the number of publications on nanofluid for every five-year period since 1995. It can be clearly seen that the intensity of research interest for nanofluids has been snowballing. Since the early 1990s, a large part of researches on nanofluids emphasized the determination of nanofluids' thermophysical and rheological properties [14, 16, 17], and their performance evaluation for various internal flow industrial applications such as heat exchangers, heat pipes, mini- and microchannels and thermal energy storage systems [18].

In single-phase convective heat transfer applications, the performance of a heat transfer fluid is highly dependent on the flow regime that is namely, laminar, transitional and turbulent. The points where the flow becomes to deviate from the laminar condition and the flow becomes fully turbulent are called transition onset and turbulence onset, respectively. Between these two points, the flow state is referred to as transitional, and the evolution of initially laminar flow into a fully developed turbulent flow is referred transition from laminar to turbulent. In a flow field, accurate prediction of transition onset and turbulence onset locations is highly important for engineers and scientists in many respects, because the laminar-to-turbulent transition separating turbulent and laminar regimes from each other can be attributed to being responsible for various physical phenomena. For example, the pressure drop and heat transfer coefficient in the turbulent flow region are much higher than the laminar state due to mixing. However, in heat transfer enhancement studies, researchers desire to augment the heat transfer coefficient with the minimum pressure drop penalty. Therefore, promoting the laminar-to-turbulent transition is desired to enhance the heat transfer rate in heat transfer augmentation researches. Besides, there are various fields such as aerodynamics where researchers want to delay the laminar-to-turbulent transition to reduce the overall drag which leads to reduce fuel consumption and the emissions released into the atmosphere and to increase the performance of vehicles. Even though the Reynolds number is used as an indicator of flow state, there are other factors that affect the laminar-to-turbulent transition such as surface imperfections, free stream turbulence intensity and adverse pressure gradient [20, 21]. Considering the above-mentioned reasons, to understand, forecast and control the laminar-to-turbulent transition of nanofluid flows in internal flow, it is necessary to examine the flow and heat transfer features of nanofluids within the transition flow region. However, the literature consists of experimental, numerical and theoretical studies aiming to assess the characteristics of different types of nanofluids in various engineering applications that have been conducted either in laminar or fully turbulent flow conditions. Furthermore, the number of studies that cover the transition flow region range in the internal flow is rather limited despite its above-mentioned importance in engineering applications [2, 22, 23, 24]. Figure 2 presents some statistics about the publications on the laminar-to-turbulent transition of nanofluid flows.

Figure 2 presents that the amount of publications at the laminar-to-turbulent transition condition of nanofluid flows in internal flow conditions is rather limited, although the

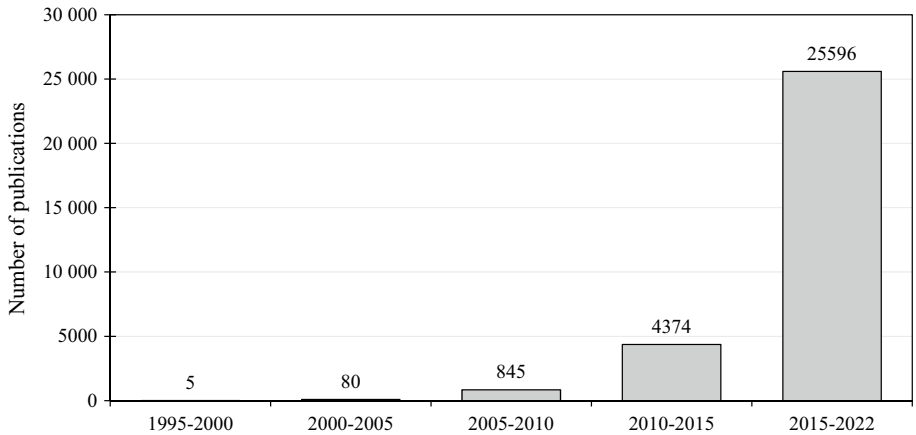

Fig. 1 Publication rate in the nanofluid area gathered through Web of Science (WOS) scan with nanofluid keyword [19]

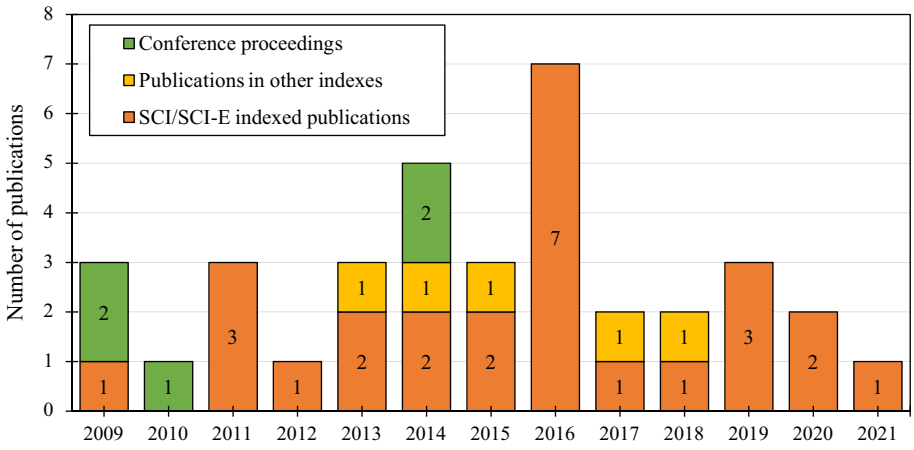

Fig. 2 Statistical distribution about the publications on the laminar-to-turbulent transition of nanofluid applications using WOS and Google Scholar scan

importance of the topic in engineering applications is mentioned above. Moreover, these publications about the topic have some deficiencies such as lack of optimization, obscure free stream turbulence intensity, low number of data points and unclear transition region in presented graphs. Although there exists one review paper about this topic in the literature [25], it includes the heat transfer performance of various fluids in smooth and enhanced tubes but not only dedicated to the transition of nanofluid flows. Since that study is not a specific work to investigate nanofluid flow in the transition region, only two articles have been reviewed and therefore provides a limited projection on the subject. To the best of the authors' knowledge, the literature has no comprehensive survey on nanofluid flows in the transitional flow region for internal flow conditions to date. Therefore, the present review aims to draw attention to this gap in the literature and to critically survey the studies conducted on this topic so far. In this context, a total of 36 publications have been reviewed aiming to determine the current research about the topic. The organization of this manuscript is listed as follows: Part 2 presents the review of application areas in the reviewed studies. Section 3 explains the characteristics of nanofluids used in the reviewed publications. In Part 4, the friction factor and heat transfer coefficient performance of nanofluids within the transition flow region for internal flows are reported including the Nusselt number and friction factor correlations. Part 5 discusses the influence of nanoparticle addition to base fluids on the delay or promotion laminar-to-turbulent transition in internal flow conditions. Finally, Sect. 6 presents the conclusions drawn from this study and recommendations for the direction of future research in this field.

Overview of application areas

This section is devoted to the applications handled in the reviewed studies. The dimensions of the experimental test rig, the type of the problem, the boundary conditions, the Reynolds number range and the method of analysis are provided in Table 1 for the nanofluid internal flows in the laminar-to-turbulent transition region studies in the literature. It can be seen from the data in Table 1 that thirty studies examined the forced convection problem, whereas only two studies analyzed the mixed convection problem. In addition, three studies have attempted to discuss the hydrodynamic characteristics of nanofluid flows in the laminar-to-turbulent transition region. The boundary conditions are critical in the analysis of heat transfer and fluid flow studies. There are two types of boundary conditions encountered in convection heat transfer problems, namely constant wall temperature and constant heat flux. In constant heat flux boundary situation applications, the aim is generally to determine the temperature distribution of the surface. For instance, an electrically heated surface and a pipe in various types of heat exchangers with a constant heat flux applied on its surface have uniform heat flux boundary conditions. In other respect, the constant wall temperature boundary condition is generally utilized in phase change applications. As presented in Table 1, most of the researchers have employed the constant heat flux situation in their studies. The reason for this can be attributed that most studies investigated the nanofluid flow for heat exchanger applications. Some studies also investigated the nanofluid flow in transition region using micro-scale test sections in order to examine heat removal characteristics in electronic cooling applications. The minimum Reynolds number was tested as 100, whereas the maximum Reynolds number value was 16,000 in experimental studies about the topic. In numerical studies, a broad range of Reynolds number from 250 to 40,000 was examined. The surface roughness is a significant parameter that affects the heat transfer and friction factor characteristics in internal flow.

Table 1 An overview of the applications handled in the reviewed papers

Application	Dimensions	Problem type	Boundary condition	Re		Analysis method	Refs.
				Lower	Upper		
Circular copper tube with and without twisted tape inserts	$d = 0.019$ m, $L_T = 1.5$ m, $L = 3.0$ m	FC	UHF	3500	8500	Exp.	[22]
Double pipe heat exchanger (counter flow)	$d_i = 4.3$ mm, $d_o = 10.5$ mm, $L_T = 2.94$ m	FC	CST	900	12,000	Exp.	[26]
Circular copper tube with and without wire coil inserts	$d = 4.85$ mm, $L_T = 1.2$ m, $L = 2.0$ m	FC	UHF	2500	5000	Exp.	[27]
Circular stainless steel minichannel	$d = 1.09$ mm, $L = 306$ mm	FC	UHF	600	4500	Exp.	[28]
Circular conduit with helical screw tape inserts	$d = 10$ mm, $L = 1.0$ m	FC	UHF	2500	5000	Exp.	[29]
Circular conduit with and without twisted tape inserts	$d = 0.014$ m, $L = 2.0$ m	FC	UHF	1000	10,000	Exp.	[30]
Copper tube	$d = 5.16$ mm, $L_T = 1.0$ m, $L = 1.5$ m	FC	UHF	1000	8000	Exp.	[2]
Aluminum multiport minichannel flat tube composed of 8 parallel independent rectangular minichannels	$W = 2.82$ mm, $H = 1.19$ mm, $L = 400$ mm (each)	FC	UHF	100	6100	Exp.	[31]
Circular copper tube and with and without helical inserts	$d = 0.014$ m, $L = 1.7$ m	FC	UHF	2500	10,000	Exp.	[32]
Circular copper tube with and without helical twisted tape inserts	$d = 10.5$ mm, $L_T = 1.0$ m, $L = 2.0$ m (Calming section made of PVC having same d.)	FC	UHF	2400	5600	Exp.	[33]
Copper pipe	$d = 8$ mm, $L = 2.0$ m	FC	UHF	800 900	1700 3000	Exp.	[23]
A tube in tube counter flow heat exchanger	$d_i = 4.3$ mm, $d_o = 10.5$ mm, $L_T = 2.97$ m	FC	CST	500	10,000	Exp.	[34]
Rectangular channel with and without staggered dimples or protrusions	$W = 125$ mm, $H = 10$ mm, $L = 245$ mm	FC	UHF	1000	40,000	Num.	[35]
Copper tube	$d = 9.52$ mm, $L = 0.8$ m	FC	UHF	500	3000	Exp.	[36]
Twin tube heat exchanger	$d_i = 8$ mm, $d_o = 15$ mm, $L_T = 0.930$ m	FC	CST	1000	6000	Exp.	[37]
Brass tube	$d = 5$ mm, $L_T = 1.045$ m, $L = 3.545$ m	HD	IST	800	12,000	Exp.	[38]
Multiport minichannel flat tube composed of 11 parallel independent rectangular minichannels	$W = 1.99$ mm, $H = 2.08$ mm, $L = 400$ mm (each)	FC	UHF	143	5308	Exp.	[39]
Stainless steel tube	$d = 4.57$ mm, $L = 1.0$ m	FC	UHF	700	4500	Exp.	[40]
Inclined pipe	$d = 0.019$ m, $L = 1.0$ m	FC	UHF	2300	10,000	Num.	[24]
Stainless steel horizontal minichannel	$d = 3.5$ mm, $L_T = 2.4$ m, $L = 2.8$ m, $\varepsilon = 3\ \mu m$	FC	UHF	300	8000	Exp. & Num.	[18]
Rectangular channel	$W = 8$ mm, $H = 5$ mm, $L_T = 450$ mm, $L = 1.15$ m	FC	UHF	200	7000	Exp.	[41]
Tube with different entrances	$d = 14.8$ & 17.7 mm, $d_{in} = 140$ mm, $L_T = 5$ m, $L = 7.4$ m	FC	CST	500	13,000	Num.	[42]
Copper tube	$d = 5$ mm, $L = 1.1$ m	FC	UHF	2500	5000	Exp.	[43]
Pipe	$d = 16$ mm	FC	UHF	2000	10,000	Exp.	[44]
Circular pipe	$d = 0.019$ m, $L = 1.0$ m	FC	UHF	2300	10,000	Num.	[45]
Backward-facing step	$d_{in} = 12.7$ mm, $d_{out} = 25.4$ mm, $L_{in} = L_{out} = 0.8$ m, $ER = 2$	FC	UHF	2000	16,000	Exp.	[46]
Copper cylindrical pipe	$d = 15$ mm, $L = 1.0$ m	FC	UHF	1500	5000	Exp.	[47]

Table 1 (continued)

Application	Dimensions	Problem type	Boundary condition	Re		Analysis method	Refs.
				Lower	Upper		
Tube heat exchanger	N/A	FC	N/A	2500	6000	Exp.	[48]
Stainless steel pipe	$d = 6.8$ mm, $L_T = 0.61$ m, $L = 1.81$ m	HD	IST	500	5000	Exp.	[49]
Microchannel	$d_h = 301$ & 212 μm, $L = 60$ mm, $\varepsilon = 69$ & 80 nm	HD	IST	200	3000	Exp.	[50]
Pipe	$d = 0.019$ m, $L = 1.0$ m	FC	UHF	250	12,000	Num.	[51]
Circular copper pipe	$d_{in} = 6$ mm, $L_T = 1.5$ m, $L = 2.1$ m	FC	UHF	1400	4000	Exp.	[52]
Copper circular tube	$d_{in} = 4.4$ mm, $d_{out} = 5.0$ mm, $L_T = 41.4$ cm, $L = 1.414$ m	FC	UHF	500	4500	Exp.	[53]
Stainless steel circular minichannel	$d_{in} = 1.09$ mm, $L = 306$ mm	FC	UHF	600	4500	Exp.	[28]
Twin circular jets	Circular target plate (having radius of 10 cm and thickness of 5 mm	FC	UHF	400	2000	Exp.	[54]

Abbreviations used in the table are *UHF* uniform heat flux, *CST* constant surface temperature, *IST* isothermal, *HD* hydrodynamic, *FC* forced convection, *Exp.* experimental, *Num.* numerical, *ER* expansion ratio and *N/A* Not available. In the table, d, L, W, H, and ε are diameter, length, width, height, and surface roughness, respectively. Subscripts, T, i, o, in, out, and h denote test section, inner tube, outer tube, inlet, outlet, and hydraulic, respectively

However, the surface roughness influence on the friction factor and Nusselt number was not examined. In the remaining reviewed papers, the researchers either used smooth test sections or did not state the roughness of the tube. The test rig design has a major role in experimental studies for the accuracy of measurements, reduction in data and discussion of the results in a proper way. The experiments are needed to be carried out in the conditioned environment, particularly when conducting experiments in turbulent and transition regions due to the instabilities which affect the laminar-to-turbulent transition. The calming section is generally introduced before the test section to have hydrodynamically and thermally fully developed flow conditions in internal flow experiments. In simultaneous developing flow conditions where the flow is hydrodynamically and thermally developing, the temperature and velocity slope near the wall of the pipe are higher in comparison with the fully developed flow conditions. As can be seen from Table 1, some researchers utilized calming section before the test section and some of them conducted test under developing conditions. It should be finally noted that Table 1 provides the information on the applications, test section details, boundary conditions and the Reynolds number range in the studies of nanofluid flow in the transition region which is expected to help the researchers who want to establish an experimental setup.

Nanofluids

The type of nanofluid suspensions is one of the most important parameters in experimental studies due to different stability features and thermo-hydraulic characteristics of the suspension according to the desired application. Tables 2 and 3 illustrate the information on nanoparticle type, base fluid type, nanoparticle concentration and size, surfactant type and concentration, the preparation technique of nanofluids, the thermophysical property determination method and the numerical approaches in the reviewed studies on the laminar-to-turbulent transition. Table 2 shows the nanofluids were prepared with two-step methods in most of the papers. The reason behind this situation is that the two-step method is very suitable for large scale nanofluid preparation with its economical feature [48]. Some researchers used surfactant such as SDBS, SDS, nitric acid, GA powder, H_2SO_4–HNO_3 mixture and PVP K30 to reduce sedimentation and improve stability of nanofluids. The base fluid was generally considered as water and deionized water, whereas the metallic type nanoparticles such as Al_2O_3, and CuO was preferred in the reviewed articles due to their high thermal conductivity. A broad range of nanoparticle size and concentration in the base fluid was utilized in the reviewed studies as can be seen from Table 2. It can be stated that the rise of the concentration of the nanoparticle within the base fluid does not always enhance the heat transfer rate because of the clustering and sedimentation of nanoparticles [2, 55].

Duangthongsuk and Wongwises [55] tested TiO_2/water nanofluids. The authors found that the heat transfer rate

Table 2 Summary on the nanofluids used in the reviewed papers

Nanoparticle	Base fluid	Preparation method	Particle concentration	Particle size	Surfactant	Surfactant concentration	Refs.
Al_2O_3	DW	Two-step	0.02%, 0.1%	47 nm	SDBS	1/10 of nanoparticles (mass)	[22]
Ag	DIW	Two-step	0.3%, 0.6%, 0.9%	~ 80 nm			[26]
Al_2O_3	DW	Two-step	0.1%	43 nm			[27]
γAl_2O_3	DIW	Two-step	1%, 2%, 3.5%, 5%	Measured 135 nm Catalogue 40 nm	A trace amount of nitric acid was added to adjust the pH value to 3.0		[28]
Al_2O_3, CuO	W	Two-step	0.1%	Al_2O_3: 40–50 nm (avg: 43 nm) CuO: 27–37 nm (avg: 30 nm) Measured			[29]
CuO	W-PG (70:30%)	Two-step	0.025%, 0.1%, 0.5%	<50 nm			[30]
MWCNT	DW	Two-step	0.33%, 0.75%, 1.0%	Outer diameter of 10–20 nm Inner diameter of 3-5 nm length of 10–30 μ*m*	GA	1% mass MWCNT 0.25% mass GA	[2]
TiO_2	W	Two-step	For $d_p = 10$ nm; 0.005%, 0.01%, 0.1%, 0.5%, 1% For $d_p = 30$ & 50 nm; 0.005%, 0.01%, 0.1%	Nominal diameters 10, 30, and 50 nm. Measured 45, 80, and 130 nm.			[31]
CuO	W-PG (70:30%)	Two-step	0.025%, 0.1%, 0.5%	Average <50 nm			[32]
Al_2O_3, MWCNT	DIW	Two-step	0.15%, 0.45%, 0.60%, 1%				[33]
ZnO	W-EG (50:50%)	Two-step	1%, 2.5%, 5% (mass)	Declared 40–100 nm. 170 nm (after 10 days)			[23]
Ag	W-EG (70:30%)	Two-step	0.05%, 0.1%, 0.15%, 0.3%, 0.45%	Declared <100 nm Measured 30–90 nm	SDS	Half of the volume fraction of silver	[34]
Al_2O_3	W		0%, 3%, 6%, 9%	30 nm diameter			[35]
Al_2O_3, CuO	W	Two-step	0.1% to 0.5%	Mean diameter 40 nm			[36]
ZnO	W-EG (50:50%)	Two-step	0% to 5% (mass)				[37]
SiO_2	DW		0.5% to 2%	25 nm and 100 nm			[38]
SiC, Al_2O_3	W	Two-step	0.001%, 0.005%, 0.01%, 0.1%, 1%		Cetyltrimethylammonium bromide used as dispersant		[39]
Al_2O_3, CuO	DIW	Single-step	0.20%, 0.30%, 0.50%		SDBS	0.10% mass for Al_2O_3 0.15% mass for CuO	[40]
Al_2O_3, TiO_2	W		6%	10 nm			[24]
Al_2O_3	IPA		0.387%, 0.992%, 3.12%, 4.71% (mass)	Catalogue 50 nm Measured DLS 75 nm & ST 82 nm			[18]
γAl_2O_3	DIW	Single-step	0.3%, 0.5%, 1%	30 nm			[41]
Al_2O_3, CuO	W		0%, 1%, 2%, 3%, 4%	35 nm and 70 nm			[42]
Fe_3O_4	DIW		0.05%, 0.16%, 0.24% (m/m)				[43]
TiO_2	W-EG (60:40%)	Two-step	0.5%, 1.0%, 1.5%				[44]
TiO_2	W		2%, 4%, 6%	10 nm and 30 nm			[45]
HCFLG	DIW		0.01%, 0.005%, 0.001% (mass)		GA	0.5:1	[46]

Table 2 (continued)

Nanoparticle	Base fluid	Preparation method	Particle concentration	Particle size	Surfactant	Surfactant concentration	Refs.
SiO_2	DW	Two-step	0.5%, 0.75%, 1.5%, 2%, 3%, 5%	12 nm (average)			[47]
TiO_2	DIW	Two-step	0.1%, 0.25%, 0.5%, 0.75%	diameter 12 nm			[48]
MWCNT	W-GLYC (45:55% mass)	Two-step	100 ppm	110–170 nm diameter 5-9 *μm* lengths	PEG SDS		[49]
Al_2O_3	DIW		0.25%				[50]
γAl_2O_3	W	Singe-step	0.25%	135 nm	A trace amount of nitric acid was added to adjust the pH value to 3.0		[28]
Al_2O_3, TiO_2	W		1%, 2%, 3.5%, 5%	100 nm			[51]
γAl_2O_3	DIW		0.75%, 1.5%, 2.5%, 3.5%, 5% (mass)	10 nm			[53]
Al_2O_3	DIW	Singe-step	0.05, 0.1, 0.15, 0.2, 0.25 kg m^{-3}				[54]
Graphene	DW	Two-step	0.025%, 0.1%, 0.2% (mass)	Graphene nanoplatelets 5–10 nm thickness 5–10 μ*m* lateral size	PVP K30	1:1 with respect to graphene mass	[52]

MWCNT multi-walled carbon nanotubes, *HCFLG* highly crumpled few-layer graphene, *W* water, *DW* distilled water, *DIW* deionized water, *EG* ethylene glycol, *PG* propylene glycol, *IP* isopropanol, *GLYC* glycerin concentrations in the table are in volume unless otherwise stated. *mass avg* average, d_p nanoparticle diameter, *ST* spectral turbidimetry, *DLS* dynamic light scattering, *SDBS* sodium dodecylbenzene sulfonate, *SDS* sodium dodecyl sulfate, *PEG* polyethylene glycol, *GA* Gum arabic

increased about 26% at the volume concentration of 1%, whereas the heat transfer rate decreased by 14% at the volume concentration of 2%. Another important feature is the size of the nanoparticles. A number of researchers used catalogue values for the size of the nanoparticles. However, this approach is not suitable since the effective particle size can be considerably different than the specified by the seller.

Liu and Yu [28] measured the effective particle size in 15-minute intervals over a period of 2 h to reveal the dependence of effective particle size on the sonication duration using the DLS technique. They reported that the nanoparticle size decreases dramatically from 186 nm within the first 30 min and reached a constant value of 135 nm at remaining 1.5 h. They also stated that the actual particle size (135 nm) is significantly larger than the specified by the supplier which was 40 nm.

In the research of Nikulin et al. [18], it was revealed that the sizes of Al_2O_3 nanoparticles are 75 nm and 82 nm measured by DLS and ST techniques, respectively, whereas the manufacturer value was less than 50 nm.

The determination of thermophysical features of nanofluids is another significant measure. In the literature, it is observed that the thermophysical properties were measured in some researches, and they were determined with empirical correlations in some other researches, see Table 3. Although the empirical correlations are generally based on the concentration of nanoparticles in base fluids, there are also some correlations considering both concentration and temperature to evaluate thermophysical properties. On the other hand, some researchers measured thermophysical properties of nanofluids for operating temperature range and concentration and found good agreement with the proposed empirical correlations. The detailed information is found in Table 3 on the determination of nanofluids' thermophysical properties in the reviewed studies.

Pressure drop and heat transfer characteristics

Many studies advised that heat transfer and fluid flow equipment should be designed and operated out of the transition flow region because of the unstable and chaotic fluid motion and large pressure drop fluctuations. However, the studies over the past decade stated that the pressure drop and heat transfer features and laminar-to-turbulent transition occur smooth and stable in the transitional flow regime [56, 57, 58]. Hence, most of the heat transfer equipments such as HVAC systems and heat exchangers in nuclear power plants and concentrated power plants have started to run within the transition flow region because it is possible to obtain a higher heat transfer rate with the least pressure drop penalty in comparison with the turbulent and laminar flow regions.

Table 3 Determination methods of the thermophysical and rheological properties in the reviewed papers

Refs.	Viscosity		Density		Thermal Conductivity		Specific Heat	
	Calculated	Measured	Calculated	Measured	Calculated	Measured	Calculated	Measured
[22]		×	×			×	×	
[26]		×	×			×	×	
[27]		×	×			×	×	
[28]		×	×			×	×	
[29]		×	×			×	×	
[30]	×		×		×		×	
[2]		×	×			×	×	
[31]		×	×			×	×	
[32]		×	×			×	×	
[33]		×	NA			×	NA	
[23]		×	×			×	×	
[34]		×		×		×		×
[35]	×		×		×		×	
[36]	×		×		×		×	
[37]		×		×		×	×	
[38]	NA		NA		NA		NA	
[39]		×	×		×		×	
[40]	×		×		×		×	
[24]	×		×		×		×	
[18]		×		×		×		×
[41]		×	×		×		×	
[42]	×		×		×		×	
[53]		×	×		NA		×	
[54]		×		×		×		×
[52]		×	×			×	×	
[43]	NA		NA		NA		×	
[44]	NA		×			×	×	
[45]	×		×		×		×	
[46]		×		×		×		×
[47]		×	NA		×		×	
[48]		×	NA			×	NA	
[49]		×		×	NA		NA	
[50]	×		×		NA		NA	
[28]	×		×		×		×	
[51]	Numerical study with discrete phase approach							

In the table, N/A corresponds not available

These methods provided mass flux reduction over the heat transfer surfaces, and therefore, heat transfer devices have begun to be operated in the lower Reynolds number span. Furthermore, nanofluids have started to be utilized as heat transfer fluids instead of conventional fluids for many years. For these reasons, more design information is needed for nanofluids flow within the transition region. This section focuses on presenting pressure drop and heat transfer performances of nanofluids in the transition region. The effects of parameters such as nanoparticle concentration on the pressure drop and heat transfer features and the performances of nanofluids in comparison with the base fluids are also discussed. In this scope, firstly, experimental studies are reviewed. Secondly, numerical studies on the nanofluid flow within the transitional regime are presented. Finally, the pressure drop and heat transfer correlations developed for the transition region are detailed.

Experimental studies

Selvam et al. [34] conducted experiments to examine the convective pressure drop and heat transfer characteristics

of Ag–deionized EG/water nanofluids at various volumetric concentrations (0.05–0.45%), nanofluid inlet temperatures (35 and 45 °C) and Reynolds numbers (500–10,000). The results revealed that the pressure drop and heat transfer rate increased as the Reynolds number and particle concentration was increased, see Fig. 3a, b. The improvement in the heat transfer rate was more noticeable when the nanofluid inlet temperature was 45 °C. Moreover, the pressure drop and the heat transfer rate of nanofluids were greater than the base fluid. Accordingly, the authors identified an optimum concentration value of 0.15% for the use of Ag nanoparticles in the water–EG mixture base fluid. It was also found that the minimum and maximum uncertainty of the convective heat transfer coefficient in the nanofluid was 2–7% in the experiments. Similar heat transfer results were also reported by by Asirvatham et al. [26]. They performed experiments with deionized water–Ag nanofluids with different volumetric concentrations in the transitional regime.

The heat transfer characteristics of ZnO–water/EG nanofluids in the transition regime have been studied by Cabaleiro et al. [23] and Li et al. [37]. Cabaleiro et al. [23] carried out experiments in a horizontal copper pipe for three different mass concentrations (1, 2.5, 5%) in the Reynolds number range between 800 and 3000. They analyzed the thermal properties of nanofluids using the Mouromtseff number and proposed that the nanofluid with 1% mass concentration is expected to present the highest thermal performance. However, the experiments showed that the nanofluid with 1% mass concentration did not exhibit heat transfer enhancement compared to the base fluid in laminar and transition regions as presented in Fig. 4. It should be noted that the authors presented this finding at the fixed Reynolds number of 800 and they did not represent the variation in the Nusselt number with the Reynolds number.

Li et al. [37] conducted experiments in a twin tube heat exchanger for three mass concentrations (1, 2.5, 5%) in the transitional flow region ($1000 \leq Re \leq 6000$). Contrary to Cabaleiro et al. [23], they reported that the nanofluid with 2.5% concentration had higher Nusselt number compared to base fluid and the enhancement increased with the increase in Reynolds number, see Fig. 5a. However, the Nusselt number of nanofluid with 5% concentration was lower than the base fluid. This is probably due to the sedimentation and agglomeration of the nanofluids on the heater surface for higher concentrations which deteriorates the heat transfer rate. Furthermore, the authors found that the pressure drop proportionally increased in turbulent flow regime, whereas there was no significant increase in the laminar flow regime as shown in Fig. 5b. It should be noted that the uncertainties of experimental parameters were not reported by the authors, and thus, it is hard to draw an exact conclusion.

In another study, Mangrulkar et al. [36] evaluated the convective heat transfer performances of Al_2O_3–water and CuO–water nanofluids within a horizontal copper tube for a wide range of volumetric concentrations (0.1–0.5%) and Reynolds number (500–3000). It was found that both nanofluids exhibited better heat transfer characteristics compared to pure water in laminar and transitional flow regimes. The heat transfer coefficient of nanofluids increased with the Reynolds number and volumetric concentration. On the other hand, the heat transfer coefficient of CuO–water nanofluid was slightly higher than the one for the Al_2O_3–water nanofluid. Singh et al. [50] investigated hydrodynamic characteristics of Al_2O_3-deionized water in two rectangular microchannels having the same heated length and different

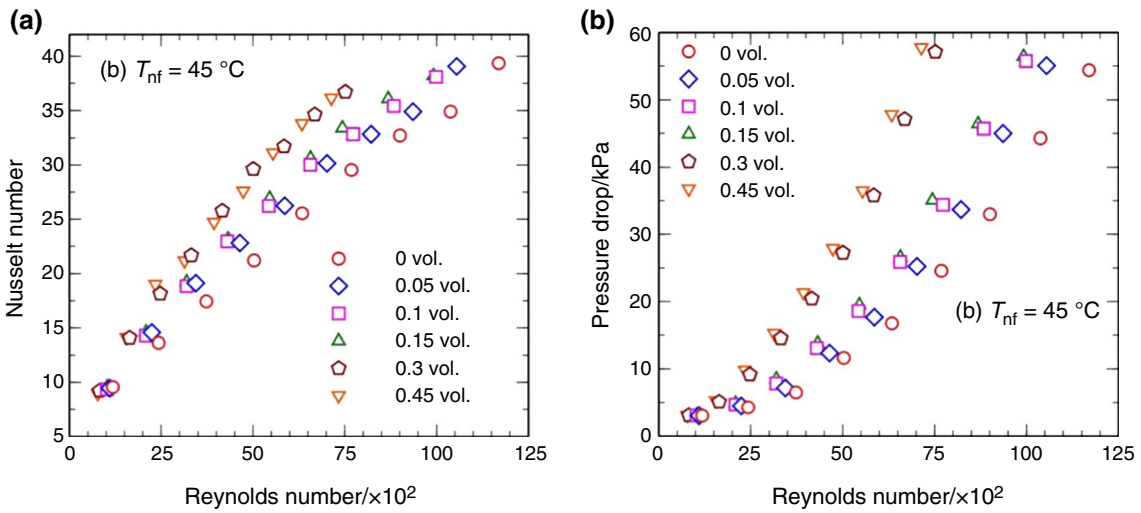

Fig. 3 Results of the experiments in transition region presented by Selvam et al. [34], for **a** heat transfer, **b** pressure drop. Reprinted with permission from Elsevier with the license number 5025290949255

hydraulic diameter for the 0.25% volumetric concentration and from 200 to 1200 Reynolds number range. They stated that the friction factor characteristics of water and nanofluid were the same. Since the authors conducted experiments for single concentration value, it is hard to compare the friction factor values of the water and the Al_2O_3–water nanofluid. Ma et al. [43] performed series of experiments to investigate the heat transfer characteristics of Fe_3O_4–water nanofluid in a horizontal copper pipe in the transition region ($2500 \leq Re \leq 5000$). Although the heat transfer coefficient of the nanofluid was detected to enhance with the Reynolds number, it decreased with the increase in the concentration and was realized to be lower than the base fluid for all cases. The findings of the Ma et al. [43] contradict the other studies in the literature. The possible reason might be the fact that the authors used empirical relation to determine the specific heat value of the nanofluid instead of measurements. In addition, they did not present the information on the determination of other thermophysical properties such as density, viscosity and thermal conductivity. The heat transfer characteristics of TiO_2 nanoparticles in pipes have been studied by Hamid et al. [44] and Logesh et al. [48]. Hamid et al. [44] compared heat transfer characteristics of TiO_2–water/EG nanofluid and the base fluid for different volumetric concentrations (0.5–1.5%) and Reynolds number range (2000–10,000). The authors reported that the heat transfer rate of the nanofluid was greater than the base fluid and increased with the increase in the Reynolds number and volumetric concentration. Logesh et al. [48] also reported similar findings with Hamid et al. [44].

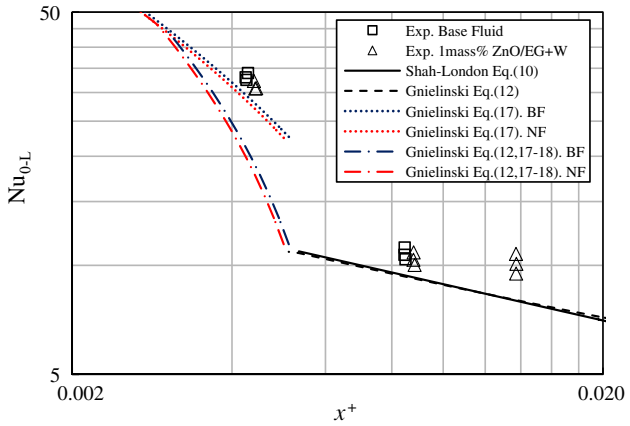

Fig. 4 Heat transfer results in transition region presented by Cabaleiro et al. [23]. Reprinted with permission from Elsevier with the license number 5025290729854

The friction factor and heat transfer features of nanofluids in enhanced geometries within the transition region have also been studied in the literature. Although the enhanced geometries provide better heat transfer performance, the accompanying friction factor penalty also becomes higher. It is also quite hard to observe laminar-to-turbulent transition in enhanced pipes. Suresh et al. [29] investigated the friction factor and heat transfer features of Al_2O_3/water and CuO/water nanofluids in a copper conduit with tape inserts (twist ratio = 1.78, 2.44, 3) for a single volumetric concentration of 0.1% and Pecklet number ($Re \times Pr$) range ($15{,}000 \leq Pe \leq 35{,}000$). They found that the heat transfer rate was better than the one for the base fluid and enhanced as the Reynolds number and nanoparticle concentration increased with an insignificant pressure drop penalty for the plain tube, please see Fig. 6a, b. Besides, the heat transfer rate and friction factor increased with introducing helical wires to the plain tube for all cases.

Other researchers who conducted experiments with enhanced geometries in the transition region using various

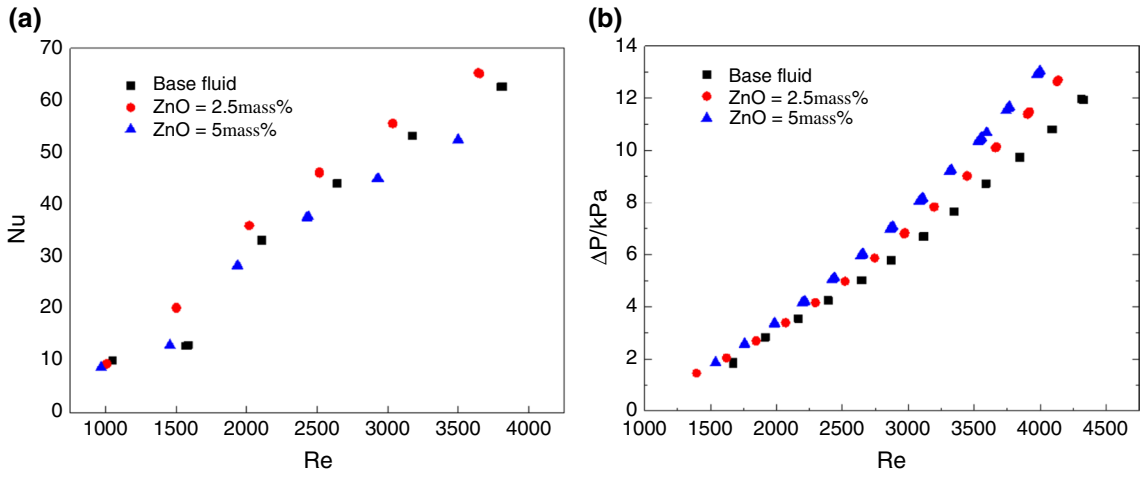

Fig. 5 Results of the experiments in transition region presented by Li et al. [37], for **a** heat transfer, **b** pressure drop. Reprinted with permission from Elsevier with the license number 5025291104163

nanoparticles reported similar results with the ones of Suresh et al. [29], see refs. [22, 27, 30, 31, 32, 33]. For instance, Sharma et al. [22] carried out an experimental study to analyze the convective heat transfer of Al_2O_3-distilled water nanofluids having different concentrations (0.02 and 0.1%) in the transition region ($3500 \leq Re \leq 8500$) using a plain tube and tubes with tape inserts having different twist ratios ($H/D = 5, 10, 15$). They found that the nanofluid flow has significantly higher convective heat transfer in the transitional flow regime compared to distilled water flow. It was also found that the heat transfer enhancement increased with the Reynolds number and nanoparticle concentration. The enhancement was more pronounced using twisted tape insert compared to the plain tube with a significant pressure drop penalty.

It should be highly emphasized that although the laminar-to-turbulent transition cannot be clearly detected on the Nu–Re and f–Re or ΔP-Re figures for the above studies even though the authors claimed that the experiments were conducted in the transition region. On the other hand, the following researchers clearly presented the laminar-to-turbulent transition in their findings. Nevertheless, none of the studies in the literature mentioned the value of the free stream turbulence intensity which has a great effect on the laminar-to-turbulent transition. Nikulin et al. [18] conducted sets of experiments to characterize the pressure drop and heat transfer behaviors of Al_2O_3-isopropanol nanofluids in a stainless steel minichannel for various nanoparticle concentrations (0.387–4.71% mass), inlet temperatures (15, 25, 35 °C) Reynolds number ($100 \leq Re \leq 10{,}000$). They reported that the friction factor values of nanofluids were higher in the laminar and turbulent flow regions, whereas it was lower in the transitional flow region, see Fig. 7b. Furthermore, the heat transfer coefficient of base fluid was almost same as the nanofluid in the laminar region, whereas it was higher in the transitional and turbulent flow regions, see Fig. 7a. They also reported that the effect of nanoparticles on the heat transfer greatly depends on the criteria selected for analysis. For instance, the authors used product of mass flow rate and specific heat capacity to evaluate the heat transfer performance of the nanofluid. They found that there is no significant effect of the nanoparticles on the heat transfer coefficient in laminar flow, while the heat transfer coefficient was deteriorated in transient and turbulent flows. The authors attributed this to the reduction in degree of turbulence. In another study, Osman et al. [41] investigated the pressure drop and heat transfer performance of Al_2O_3 -deionized water nanofluids in a rectangular channel for various volumetric concentrations (0.3–1%) in the transitional regime. It was found that the heat transfer coefficient and pressure drop penalty increased with the increase in the concentration and they were higher in the transitional flow regime compared to the turbulent flow regime, see Fig. 8a, b. Similar findings were also reported in [2] and [28].

Briclot et al. [53] performed experiments using Al_2O_3 -deionized water nanofluids (0.75-5 mass%) through circular tubes for a wide range of Reynolds number ($500 \leq Re \leq 4500$). They found that the pressure drop increased with the Reynolds number and concentration and was higher than the one for the base fluid for all cases studies. Besides, the existence of nanoparticles in the base fluid did not significantly affect the heat transfer rate in all flow regimes compared to the base fluid alone. In another study, Zhang et al. [31] studied the effects of particle diameter and volume concentrations on the heat transfer and pressure drop characteristics of TiO_2–water nanofluid in the transition

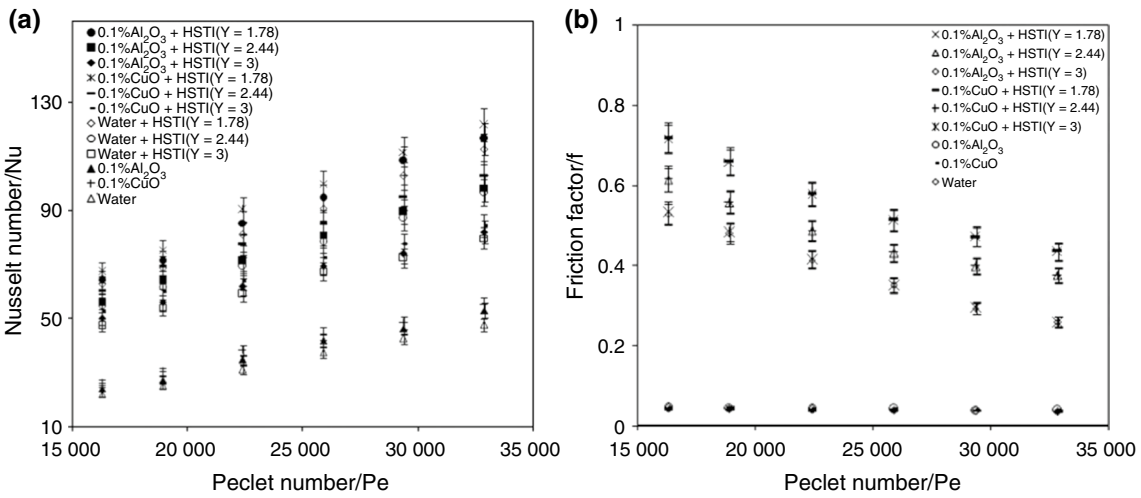

Fig. 6 Results of the experiments in transition region presented by Suresh et al. [29], for **a** heat transfer, **b** friction factor. Reprinted with permission from Elsevier with the license number 5025290842941

region ($100 \leq Re \leq 6100$). They reported that the friction factor and Nusselt number of nanofluids were higher than those of water in all flow regimes. Furthermore, the particle diameter and volume concentration had an insignificant effect on the friction factor at a given Reynolds number for the concentration of less than 0.1%. However, the friction factor was the highest and the Nusselt number was the lowest at the concentration of 0.1% for all Reynolds number range.

Table 4 summarizes the findings of all experimental studies reviewed in this article. The key remarks by the authors as well as the information on the detection of the laminar-to-turbulent transition are presented.

Numerical studies

There are only a few numerical researches regarding the nanofluid flow in the transition flow region. Generally, three approaches were used, namely the single-phase model, the multi-phase mixture model and the dispersed particle model. The single-phase model assumes the nanofluid in single phase and evaluates the thermophysical properties with empirical models, please see ref. [35]. The multiphase mixture model assumes the mean temperatures and local velocities of the phases to be equal and the interaction between nanoparticles and fluid is taken into account [24]. Furthermore, the multi-phase mixture model enables the define velocity of phases using the drift velocity concept. Xie et al. [35] performed a CFD study to reveal the effects of Al_2O_3/water nanofluid flow on heat transfer characteristics and entropy generation in a rectangular conduit with staggered protrusions and dimples. They considered four different volume fractions for the Reynolds number covering laminar, transitional and turbulent flow regions. They assumed nanofluid is under single-phase flow conditions. It was revealed that the average heat transfer entropy generation decreased at a given Reynolds number when the volume concentration was increased. The employment of nanofluid increased the average friction entropy generation at a given Reynolds number when the volume fraction was increased. Saha and Paul [24] examined the transitional flow behavior of Al_2O_3–water and TiO_2–water nanofluids flow through an inclined pipe utilizing both multi-phase and single models. Although the authors claimed that they covered the transitional regime, the Nu–Re and *f*–Re or ΔP-*Re* graphs did not exhibit the transitional flow regime behaviors. They concluded that the friction factor elevated as the Reynolds number was increased at various inclination angles. Besides, the higher inclination angles led to the higher friction factor. Furthermore, the mean heat transfer rate reduced when the Reynolds number increases in different inclination angles. In another study, Jamali and Toghraie [42] investigated the heat transfer features for the fully developed and developing flow conditions of Al_2O_3–water and CuO–water nanofluids through a conduit having different entrances in the transitional region. They found that the Nusselt number of the nanofluid and base fluid increased with increasing Reynolds number. The average heat transfer coefficient of CuO–water nanofluid augmented by increasing Reynolds number and the rate of increase in heat transfer coefficient varied depending on type and diameter of nanoparticle. The convective heat transfer coefficient of Al_2O_3 and CuO nanoparticles reduced with decreasing nanoparticle diameter. The friction factor elevated by increasing Reynolds number. The heat transfer coefficient of CuO was smaller than the one for Al_2O_3. Finally, Saha and Paul [51] employed the discrete phase model to investigate the Al_2O_3–water and TiO_2

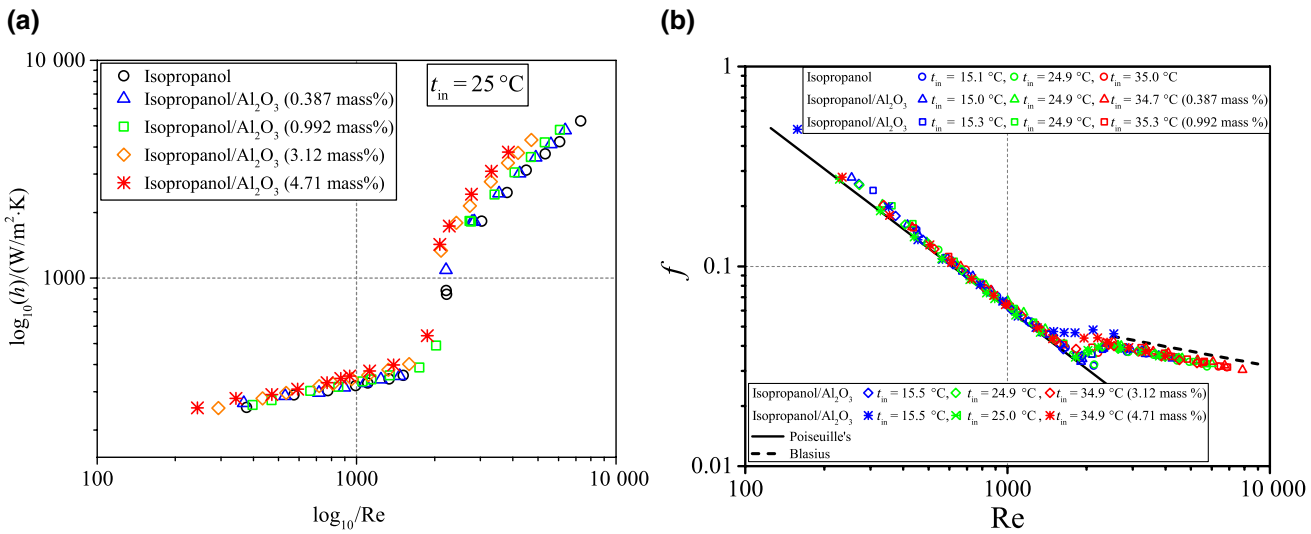

Fig. 7 Results of the experiments in transition region presented by Nikulin et al. [18], for **a** heat transfer, **b** friction factor. Reprinted with permission from Elsevier with the license number 5025290624013

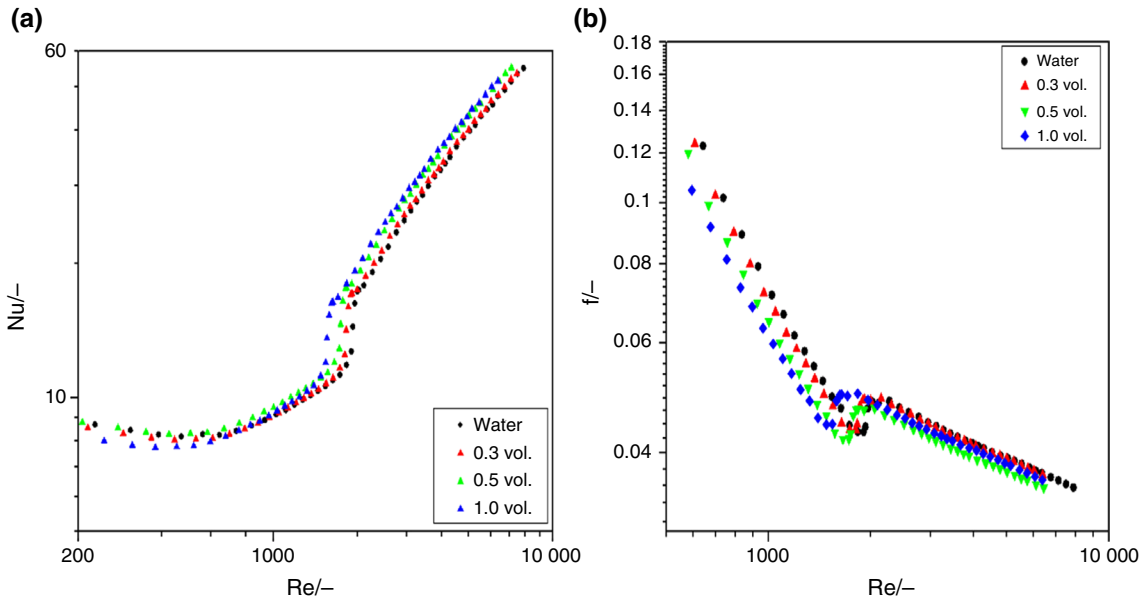

Fig. 8 Results of the experiments in transition region presented by Osman et al. [41], for **a** heat transfer, **b** friction factor. Reprinted with permission from Elsevier with the license number 5025291316472

–water nanofluid flow in a circular pipe from a Reynolds number span of 250–12,000. The numerical model was verified with the experimental data collected from the literature. The authors concluded that the discrete phase model is an excellent tool since it only requires the thermophysical properties of nanoparticles and base fluid seperately.

In all above studies, the authors determined the thermophysical properties of nanofluids using correlations from the literature in the numerical studies. Also most of them did not validate their model with the experimental data instead they validated their model with the conventional correlations such as Shah and London [59] and Gnielinksi [60]. This affects the accuracy of the results dramatically. Because the relations of Shah and London [59] and Gnielinksi [60] are validated for pure substances where they do not consider the particle fluid interaction in nanofluids. Furthermore, the turbulence models such as Transition SST, and $k-k_L-\omega$ which are suitable for transitional flows are for external flows. The coefficients in these turbulence models were calibrated for external flows. Therefore, they cannot be used for internal flows directly. The coefficients need to be calibrated before using these turbulence models for internal flows. However, in all of the above-mentioned studies, there is not any explanation about the tuning of turbulence models implying they employed the turbulence models without any modification.

Friction factor and Nusselt number correlations

This section presents the friction factor and Nusselt number relations proposed by the authors to predict friction factor and Nusselt number for nanofluid flow in turbulent, transition and laminar flow regions. Sharma et al. [22] found that the classical heat transfer equation of Gnielinski [60] within the transitional region under-predicted their experimental dataset. Accordingly, they developed a Nusselt number correlation using the experimental data under for both nanofluids and water having volumetric concentration lower than 0.1%, see Eq. (1). The proposed correlation was implemented for uniform heat flux boundary conditions. The authors experimentally measured the viscosity and thermal conductivity of nanofluids at various temperatures. But, the specific heat and density of nanofluids were determined with analytical expressions from the literature.

$$Nu = 3.138 \times 10^{-3} \mathrm{Re} Pr^{0.6} (1.0 + H/D)^{0.03} (1 + \varphi)^{1.22} \quad (1)$$

where H/D represents the twist ratio and φ is the particle volume fraction of nanoparticles in the base fluid. In another study, Asirvatham et al. [26] compared their experimental data with sets of relations from the literature. All the correlations including the correlation of Xuan and Li [61], which was developed for nanofluids, did not well predict their data. Therefore, the authors developed a correlation to forecast the Nusselt number of the experimental data for Ag–water nanofluid as can be seen from Eq. (2). The proposed correlation works under constant temperature boundary conditions. The

Table 4 Heat transfer and friction factor characteristics of nanofluid flows handled in the reviewed papers

Ref.	Detection of transition	Remarks
[2]	Yes	• The nanofluids showed better heat transfer characteristics with an additional pressure drop penalty compared to the base fluid in the transitional flow regime. • The friction factor and the Nusselt number increased as the particle concentration increased within the transitional flow region
[18]	Yes	• The nanofluids exhibited higher pressure drop and heat transfer features as the concentration and Reynolds number was increased in comparison with the base fluid at all flow regimes
[22]	No	• The nanofluid flow has significantly higher convective heat transfer rate within the transition flow region compared to the base fluid. • The heat transfer rate enhanced as the Reynolds number and nanoparticle concentration increased
[23]	No	• The nanofluid did not exhibit heat transfer enhancement in comparison with the base fluid within laminar and transition regions
[26]	No	• The heat transfer rate augmented with the concentration and the Reynolds number and it was higher than the one for the base fluid
[27]	No	• The use of nanofluids increased the heat transfer rate with negligible friction factor penalty increment as the Reynolds number was increased within the range of parameters investigated
[28]	Yes	• The nanofluids exhibited hydrodynamically and thermally developing flow characteristics within the laminar flow regime. • The pressure drop values of nanofluids were higher in the turbulent and laminar flow regions. But it was lower in the transition flow region compared to the base fluid. • The heat transfer performance of the base fluid was almost the same as the nanofluid within the turbulent and laminar flow regions. But it was greater in the transition flow region. • The Nusselt number and friction factor values of nanofluids were independent of the nanoparticle concentration in the investigated range of parameters.
[29]	No	• The Nusselt number increased, whereas the friction factor decreased as the performance factor increases
[30]	Yes	• Significant augmentation in the heat transfer rate was observed with CuO nanofluids over the base fluids, and heat transfer enhancement was linearly proportional to the nanoparticle volume concentration in the base fluid. • The friction factor penalty increment of nanofluids within the base fluid was not considerable in a smooth conduit. • The utilization of twisted tapes in CuO nanofluids enhanced the heat transfer coefficient with a little increment of friction factor, and transfer enhancement was proportional to the number of twists on inserts.
[31]	Yes	• The Nusselt number and the friction factor of nanofluids were greater than the base fluid in all flow regimes. • The particle diameter and volume concentration had an insignificant influence on the pressure drop at a given Reynolds number for the concentration of smaller than 0.1%. However, the friction factor was the highest and the heat transfer rate was the lowest at the concentration of 0.1% for all Reynolds number range.
[32]	No	• The heat transfer rate augmented as the nanoparticle concentration and the Reynolds number increased. • No considerable friction factor penalty was reported for CuO nanofluids in comparison with its base fluid.
[33]	No	• The heat transfer rate increased with the particle concentration and the Reynolds number for both nanofluids. • The *CNT*/water nanofluid showed remarkable higher Nusselt number performance in comparison with the Al_2O_3/water nanofluid for all concentrations and twist ratios.
[34]	No	• The heat transfer and friction factor increased with the particle concentration. • The heat transfer and friction factor of nanofluids were higher than the base fluid.
[36]	No	• The nanofluids showed higher Nusselt number characteristics in comparison with the base fluid in laminar and transitional flow regimes. • The Nusselt number of nanofluids enhanced as the particle volume concentration and the Reynolds number increased.
[37]	No	• The nanofluid had higher Nusselt number in comparison with the base fluid and the enhancement increased with the increase in the Reynolds number. • The friction factor proportionally elevated in turbulent flow region, whereas no considerable increase in the laminar flow regime was observed.
[38]	Yes	• The friction factor was higher for the nanofluids with higher concentration in all flow regimes. • The smaller nanoparticle size resulted in higher friction factor in all flow regimes. • The friction factor of nanofluids was higher compared to the base fluid for all flow regimes.
[39]	Yes	• The pressure drop of the nanofluids increased significantly in comparison with the base fluid. • Both nanofluids exhibited a common optimal volume concentration of 0.01% for heat transfer. • The nanofluid with a small particle size demonstrated good heat transfer capability. • The *SiC*–water nanofluid had higher Nusselt number than the Al_2O_3–water nanofluid.

Table 4 (continued)

Ref.	Detection of transition	Remarks
[40]	Yes	• Both Al_2O_3/deionized water and deionized CuO/deionized water nanofluids exhibited a considerable enhancement in Nusselt number compared to the base fluid for all flow regimes. • The friction factor was decreased as the Reynolds number as well as mass fraction of nanoparticles in the nanofluids increased. • The first law efficiency of the nanofluids enhanced for higher nanoparticle concentration and input power. • The CuO/deionized water nanofluids exhibited highest first law efficiency and Nusselt number with lowest exergy loss and friction factor.
[41]	Yes	• The heat transfer coefficient and pressure drop penalty increased with the increase in the concentration and they were greater in the transition flow region compared to the turbulent flow regime.
[43]	No	• The base fluid showed better heat transfer performance than the nanofluid.
[44]	No	• The heat transfer coefficient of the nanofluid was greater compared to the base fluid and increased with increasing particle volume concentration and the Reynolds number.
[46]	No	• The nanofluid showed superior heat transfer performance in comparison with the base fluid. • The pressure drop of nanofluid elevated with the Reynolds number and concentration and was greater for all concentration values.
[48]	No	• The Nusselt number increased significantly with concentration and the Reynolds number.
[49]	Yes	• The pressure drop in the turbulent and transition flow regions was reduced with the addition of CNT nanoparticles into the base fluid.
[50]	No	• The pressure drop characteristics of the base fluid and the nanofluid were found to be the same.
[53]	Yes	• The pressure drop increased with the particle concentration and Reynolds number and was higher than the one for the base fluid for all cases investigated. • The nanoparticles in the base fluid did not considerably influence the Nusselt number in all flow regimes compared to the base fluid.
[54]	No	• The maximum increase in the Nusselt number was around 200% at the concentration value of 0.25% and the Reynolds number value of 2000 in comparison with the base fluid.
[52]	Yes	• The rise in pressure drop for studied nanofluids did not exceed 10% in comparison with the base fluid in the laminar and turbulent flow regimes, whereas it was up to 30% for the transitional flow region. • The local Nusselt number augmentation for nanofluids at various mass fluxes and x/D=240 and x/D=120 approximately did not change with the Reynolds number. • Nanofluids had similar Nusselt numbers at a given axial conditions and Reynolds number. The average heat transfer coefficient enhancement was around 7%, 17%, and 22% for the nanofluids with 0.025%, 0.1%, and 0.2% particle concentration, respectively. • Considerable Nusselt number augmentation was observed in turbulent flow of nanofluids. • The friction factor increase was comparatively low in the turbulent and laminar flow regions. But, it was greater in the transition flow regime.

thermophysical properties of nanofluids were found with the aid of correlations existed in the literature including the own correlations of authors. The correlation enables the calculation of Nu for Ag-*water* nanofluids at wide ranges of Re, Pr, temperatures and volume concentrations. The correlation predicted the experimental data with ±10% deviation.

$$\mathrm{Nu} = 0.023\mathrm{Re}^{0.8}Pr^{0.8} + (0.617\varphi - 0.135)\mathrm{Re}^{(0.445\varphi-0.37)}Pr^{(1.081\varphi-1.305)} \tag{2}$$

Chandrasekar et al. [27] created Nusselt number and friction factor correlation for Al_2O_3water nanofluid flow in tubes with wire coil inserts based on only 16 experimental data points, see Eqs. (3) and (4). The proposed correlations were developed for transitional flow region ($2500 < \mathrm{Re} < 5000$) under constant heat flux boundary conditions. The viscosity and thermal conductivity of nanofluids were determined at various temperatures. The specific heat and density of nanofluids were determined with the correlations available in the literature. The absolute mean error between the results determined by the experimental data and the correlation was reported to be 3.2% and 2.9% for Nusselt number and friction factor, respectively. They also found that these correlations led to a highest deviation of +2% and –8% for the Nusselt numbers, and ±8% for the friction factors.

$$Nu = 0.0015\mathrm{Re}_{\mathrm{nf}}^{1.339}\mathrm{Pr}_{\mathrm{nf}}^{0.4}\left(1+\frac{p}{d}\right)^{-0.948}(1+\varphi)^{-37.18} \tag{3}$$

$$f = 164.06\mathrm{Re}_{\mathrm{nf}}^{-0.723}\left(1+\frac{p}{d}\right)^{-1.563}(1+\varphi)^{302.09}$$
$$2300 < \mathrm{Re} < 5000, \quad \varphi = 0.1\,\%, \quad 2 \le p/d \le 3 \tag{4}$$

In Eqs. (3) and (4), Re_{nf} and Pr_{nf} were calculated using effective nanofluid properties. p/d and f represent the pitch ratio over tube diameter and the friction factor, respectively. Naik et al. [30] proposed sets of the Nusselt number and the friction factor correlations for smooth tubes and tubes having twisted tapes for different Reynolds number range as presented in Eqs. (5)–(10). The measurements were conducted under uniform heat flux boundary conditions with water–propyleneglycol-based CuO nanofluids. All thermophysical characteristics of nanofluid were evaluated with the empirical relations from the literature at different temperatures.

For plain tube;

$$\begin{aligned} &\mathrm{Nu} = 0.1168\mathrm{Re}^{0.59106}Pr^{0.4}(1+\varphi)^{0.2307} \\ &1000 < \mathrm{Re} < 10000, \quad 0 < \varphi < 0.5\,\%, \quad 11 < \mathrm{Pr} < 19.52 \end{aligned} \tag{5}$$

For twisted tape inserts;

$$\begin{aligned} &\mathrm{Nu} = 0.1251\mathrm{Re}^{0.5855}Pr^{0.4}(1+\varphi)^{0.3772}\left(1+\frac{H}{D}\right)^{0.05351} \\ &1000 < \mathrm{Re} < 10000, \quad 0 < \varphi < 0.5\,\%, \quad 11 < \mathrm{Pr} < 19.52 \\ &0 < H/D < 15 \end{aligned} \tag{6}$$

For plain tube;

$$\begin{aligned} &f = 24.08Re^{-0.8456}(1+\varphi)^{0.1720} \\ &1000 < \mathrm{Re} < 2500, \quad 0 < \varphi < 0.5\,\% \end{aligned} \tag{7}$$

$$\begin{aligned} &f = 0.2753Re^{-0.2279}(1+\varphi)^{0.2129} \\ &2500 < \mathrm{Re} < 10000, \quad 0 < \varphi < 0.5\,\% \end{aligned} \tag{8}$$

For twisted tape inserts;

$$\begin{aligned} &f = 23.01Re^{-0.8436}(1+\varphi)^{0.4336}\left(1+\frac{H}{D}\right)^{0.004051} \\ &1000 < \mathrm{Re} < 2500, \quad 0 < \varphi < 0.5\,\%, \quad 0 < H/D < 15 \end{aligned} \tag{9}$$

$$\begin{aligned} &f = 0.2086Re^{-0.1946}(1+\varphi)^{0.2507}\left(1+\frac{H}{D}\right)^{0.01251} \\ &2500 < \mathrm{Re} < 10000, \quad 0 < \varphi < 0.5\,\%, \quad 0 < H/D < 15 \end{aligned} \tag{10}$$

In Eqs. (5)–(10), H is length of the tape pitch and D represents the inner diameter of the tube. Naik and Sundar [32] also proposed the Nusselt number and friction factor relations using their experimental data for smooth tube and tube having helical inserts, see Eqs. (11)–(13). The proposed correlations were developed for propylene glycol/CuO nanofluids under uniform heat flux boundary conditions. All thermophysical properties of nanofluid were evaluated using the correlations from the literature at different temperatures. The experimental Nusselt number data were predicted with a mean deviation of 5.5% and standard deviation of 6.9% with the proposed correlation. The friction factor was predicted with a mean deviation of 2.1% and standard deviation of 3.0% with the new correlation.

$$\begin{aligned} &Nu = 0.32\mathrm{Re}^{0.45}Pr^{0.48}(1+\varphi)^{0.32}\left(1+\frac{H}{D_e}\right)^{-0.3}\left(\frac{D}{D_e}\right)^{1.27} \\ &2500 < \mathrm{Re} < 10000, \quad 0 < \varphi < 0.5\,\%, \quad 6.5 < \mathrm{Pr} < 19.98 \\ &1 < D/D_e < 5, \quad 0 < H/D_e < 9 \end{aligned} \tag{11}$$

$$\begin{aligned} &f = 0.18\mathrm{Re}^{-0.18}(1+\varphi)^{0.23}\left(1+\frac{H}{D_e}\right)^{-0.09}\left(\frac{D}{D_e}\right)^{0.3} \\ &2500 < \mathrm{Re} < 10000, \quad 0 < \varphi < 0.5\,\%, \quad 6.5 < \mathrm{Pr} < 19.98 \\ &1 < D/D_e < 5, \quad 0 < H/D_e < 9 \end{aligned} \tag{12}$$

where

$$D_e = \frac{4\left[\left(\frac{\pi}{4}D^2\right) - \left(\frac{\pi}{4}d^2 + \frac{\pi}{4}t^2\right)\right]}{\pi(D+d+t)} \tag{13}$$

In another study, Khairul et al. [40] compared their experimental results with the conventional correlations such as Dittus and Boelter [62] and Duangthongsuk and Wongwises [55] reported in various studies. They found that the predicted Nusselt number of nanofluids was lower compared to the experimental Nusselt number. Consequently, they introduced the following Nusselt number correlations for Al_2O_3–water and CuO–water nanofluids as a function of Prandtl number, volumetric concentration of nanofluids and Reynolds number, see Eqs. (14)–(17). The experiments were performed under uniform heat flux boundary conditions for three particle concentrations (0.2, 0.3, and 0.5 mass%) for both of the nanofluids. property values of nanofluid were evaluated with the empirical relations from the literature. The new proposed relations predicted the Nusselt number with a maximum deviation of ±5% for all the concentrations of Al_2O_3 and CuO nanofluids for laminar flow, whereas the maximum variation was found +8% and -5% for turbulent flow regime.

For Al_2O_3–water within the laminar flow region;

$$Nu = 0.86\mathrm{Re}^{0.205}Pr^{0.33}\varphi^{0.1} \tag{14}$$

For CuO–water within the laminar flow region;

$$Nu = 1.04\mathrm{Re}^{0.205}Pr^{0.33}\varphi^{0.1} \tag{15}$$

For Al_2O_3–water within the turbulent flow region;

$$Nu = 0.033\mathrm{Re}^{0.85}Pr^{0.385}\varphi^{0.1} \tag{16}$$

For CuO–water within the turbulent flow region;

$$Nu = 0.016\mathrm{Re}^{0.957} Pr^{0.385} \varphi^{0.1} \tag{17}$$

From a numerical study, Saha and Paul [45] proposed the following correlations the highest standard deviation of error of 5% for the numerical determination of the mean Nusselt number, see Eqs. (18)–(19).The correlations were developed for TiO_2–water nanofluid flow in a tube for uniform heat flux boundary conditions. The authors determined the thermophysical properties using two methods namely single-phase model and multi-phase model.

With single-phase model;

$$Nu = 0.03930\mathrm{Re}^{0.76745} Pr^{0.24165} \left(\frac{d_\mathrm{f}}{d_\mathrm{p}}\right)^{-0.0007074} \tag{18}$$

With multi-phase model;

$$Nu = 0.037768\mathrm{Re}^{0.76536} Pr^{0.26123} \left(\frac{d_\mathrm{f}}{d_\mathrm{p}}\right)^{-0.0062903} \tag{19}$$

where $8.45 \le Pr \le 20.29$, $2300 \le \mathrm{Re} \le 10 \times 10^3$, $10 \le d_p \le 40$, $0 \le \varphi \le 6\%$. It should be noted that these correlations were obtained by regression analysis based on the authors' experimental data. Also, some correlations were developed based on very low data points. Furthermore, the correlations proposed by the authors have not been tested for other data sets, and therefore, it is quite hard to draw a general conclusion. Thus, it is needed to develop friction factor and heat transfer relations for nanofluid flow based on a wide range of parameters and universal data sets for all regimes. Moreover, some new methods such as Artificial Neural Networks (ANN) and Deep Learning (DL) can be utilized to estimate the Nusselt number and the friction factor as an alternative to correlations.

Do adding nanoparticles into base fluids delay or promote laminar-to-turbulent transition compared to base fluids?

Generally speaking, the onset of transition is observed to occur at the Reynolds number of 2300 for internal flows. However, many factors such as surface roughness, diameter of the conduit, nanofluid flow and the turbulence intensity affect the onset of transition point. On the other hand, most of these parameters were not considered in the reviewed papers. For example, only two studies employed rough test sections in the reviewed articles. Singh et al. [50] measured axial pressure variation along two rectangular microchannels having different hydraulic diameters and the same heated length to examine the influence of microchannel size and nanofluid concentration on friction factor in a range of Reynolds number of 200 and 1200. The roughness of the surface the microchannels was reported as 69 nm and 80 nm, but the influence of surface roughness on the friction factor was not examined. In another study, Nikulin et al. [18] examined the effects of isopropanol-based Al_2O_3 nanofluid flow in a horizontal circular stainless steel conduit having 2.4 m inner diameter and 3 μm surface roughness on the convective heat transfer characteristics in a Reynolds number from 300 to 8000. As mentioned earlier, the precise estimation of the transition onset is rather important in many engineering applications. For instance, the laminar-to-turbulent transition is desired to be promoted in heat transfer applications, whereas it is desired to be delayed in aerodynamics applications. In the literature, there are only a few studies concerning the effect of the nanoparticle addition into the base fluid on the transition onset. In the study of Steele et al. [49], the impacts of MWCNT addition into the water/glycerin and POE solution on the onset of transition point was investigated in a stainless steel pipe. They reported that the addition of CNT into the POE solution increased the transition onset from 2500 to about 2900 with reducing the friction factor by an average of 35%. Similarly, Liu and Yu [28] stated that the critical Reynolds number which the transition onset occurs was slightly delayed ($\mathrm{Re}_{cr} \sim 2500$) in comparison with the base fluid with the addition of Al_2O_3 nanoparticles into the base fluid. They attributed this due to the particle fluid interaction, which reduced the instabilities in the flow.

Contrarily, Meyer et al. [2] stated that the incorporation of MWCNT into the distilled water promoted laminar-to-turbulent transition. Moreover, this promotion increased as the nanoparticle volumetric fraction in the base fluid was enhanced, see Fig. 9a, b. They reported that the measured viscosity values of the nanofluids are higher in comparison with the distilled water, and therefore, the transition onset was shifted to earlier. Rudyak et al. [38], Osman et al. [41], Demirkir and Erturk [52] and Nikulin et al. [18] agreed with the findings of Meyer et al. [2]. Osman et al. [41] also stated that the early transition can be can be explained by the larger viscosity value of the nanofluid compared to the base fluid since higher viscosity provided a shift in the *f*–Re and Nu–Re figures. On the other hand, in the study of Demirkir and Erturk [52] the reason of the early transition was additional disturbance generated by the graphene nanoparticles in denser nanofluids since the nanoparticles caused microturbulence and hence helped the inertia force became more dominant. The dominant inertia force provided the induction of fluctuations at lower flow rates. In another study, Zhang et al. [31] also reported that the TiO_2–water nanofluids provided slightly earlier laminar-to-turbulent transition ($\mathrm{Re}_{cr} \sim 1800$) in comparison with the base fluid and the nanoparticle diameter had no effect on this phenomenon. This was attributed to the chaotic movement of nanoparticles within the fluid. In addition to above studies, a group of researchers found that the effect of the nanoparticle addition

into the base fluid on the transition onset was insignificant as can be presented in Fig. 10a, b, see Refs. [39, 40] and [53].

The above literature review shows that there is no agreement on the effect of nanoparticle addition into the base fluid on the laminar-to-turbulent transition. Two research groups reported that the nanoparticle addition delayed the onset of turbulence, whereas six research groups stated the opposite. Moreover, three research groups concluded that the nanoparticle addition into the base fluid had no effect on the transition onset. Please note that none of the research groups mentioned the value of the free stream turbulence intensity and surface roughness which has a great effect on the laminar-to-turbulent transition.

Concluding remarks and recommendations for future researches

An extensive synopsis of the literature review on the pressure drop and heat transfer features of nanofluid flows in the transition region for internal flows is presented. The effect of nanoparticle addition into the base fluid on the transition onset in internal flows is also discussed. Although the precise estimation of transition onset location is highly important in many fields, the number of studies covering the transition flow region for the internal flow of nanofluids is rather limited. The current state of the art is introduced by reviewing thirty-six publications about the topic. It was found that the pressure drop and heat transfer features of nanofluid flows in the transition region for internal flow conditions are still not completely understood with limited numerical and experimental studies concluding contradicting results. Possible reasons of the discrepancies might be that the experimental conditions, employed numerical model, determination of thermophysical and rheological properties and measurement uncertainties. It was revealed that some researchers did not measure thermophysical properties; instead, they used empirical correlations that may result in incorrect findings. The main results of this study can be summarized accordingly.

- Some researchers found that the heat transfer coefficient and pressure drop augmented with the increase in the Reynolds number and particle concentration in the transition regime and were higher than the ones for base fluid; some others reported that the nanofluid did not exhibit heat transfer enhancement compared to base fluids for all flow regimes.
- Some researchers claimed that they conducted experiments in the transition flow region although the laminar-to-turbulent transition cannot be clearly detected from the Nu–Re and f–Re or $\Delta P - \mathrm{Re}$ figures.
- None of the studies in the literature mentioned the value of free stream turbulence intensity which has a great effect on the laminar-to-turbulent transition.
- Even though surface roughness has considerable influence on the transition onset, some researchers did not state the roughness of the test section.
- The Nusselt number and friction factor correlations introduced by the authors for the use in nanofluid flows in the transitional flow regime have either very low data points or have not been tested for universal data sets. Therefore, a general conclusion cannot be drawn.
- The researchers generally used turbulence models in numerical studies for the transitional flow which are suitable for external flows and are needed to be calibrated

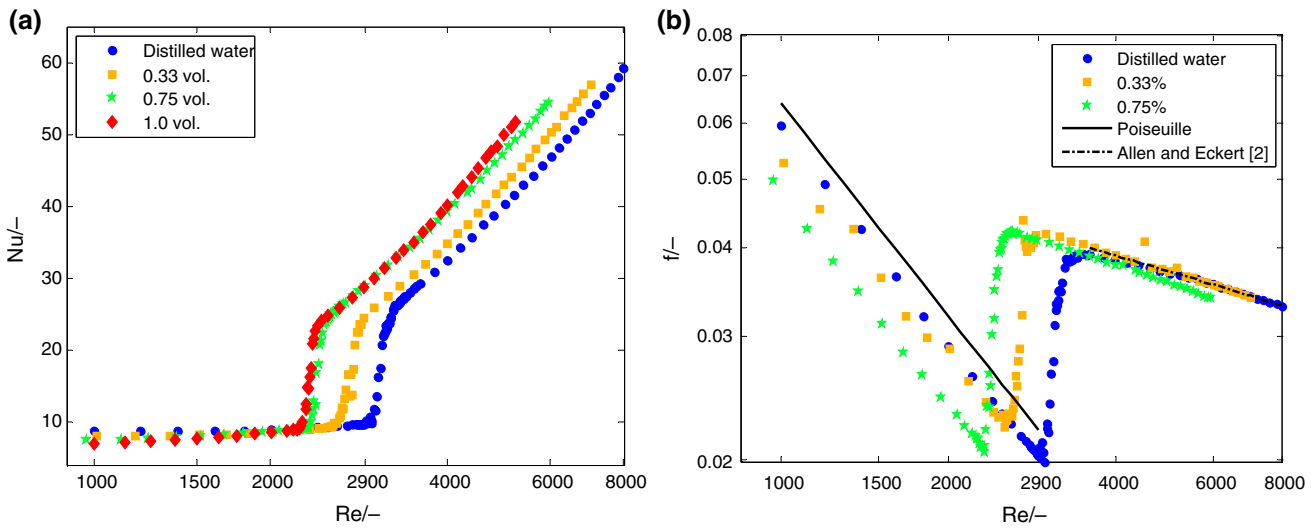

Fig. 9 Results of the experiments in transition region presented by Meyer et al. [2], for **a** heat transfer, **b** friction factor. Reprinted with permission from Elsevier with the license number 5025290352840

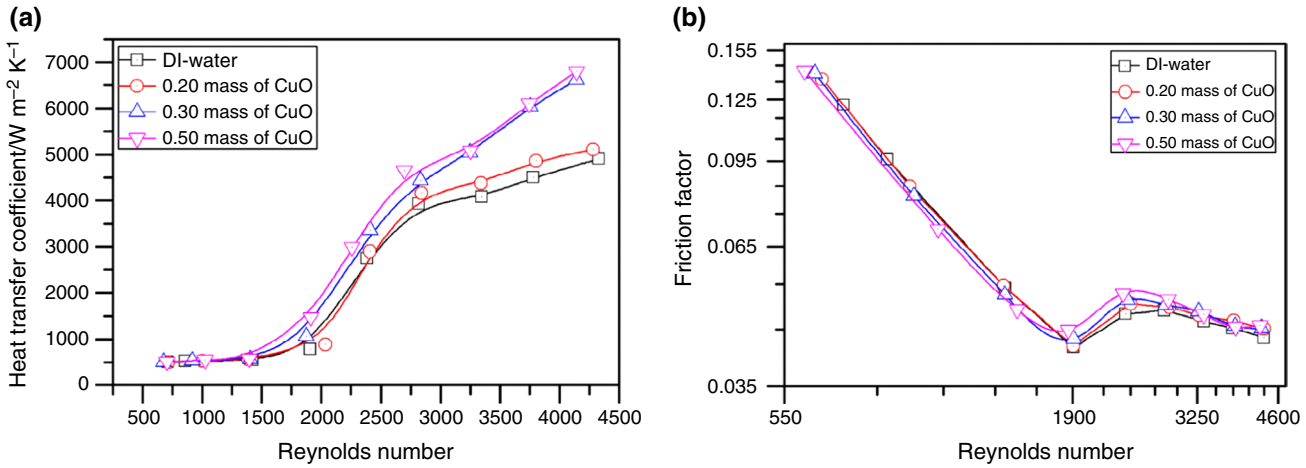

Fig. 10 Results of the experiments in transition region presented by Khairul et al. [40], **a** heat transfer, **b** friction factor. Reprinted with permission from Elsevier with the license number 5025291205236

when used for internal flows. The researchers did not mention any explanation about the calibration of turbulence models used.

- There is no agreement on the influence of nanoparticle addition into the base fluid on the laminar-toturbulent transition. Two research groups reported that the nanoparticle addition delayed the onset of turbulence, whereas six research groups stated the opposite. Three research groups concluded the incorporation of the nanoparticles within the base fluid had no effect on the transition onset. More research is necessary to investigate the influence of nanoparticle addition into the base fluid on the laminar-to-turbulent transition.

Based on the discussion of available literature, some recommendations can be made for future studies about the topic.

- The experiments on laminar-to-turbulent transition of nanofluid flows should be conducted in a well- designed, well-established, and controlled experimental setup in order to obtain reliable results. Calming section length, mixer employment, control of fluid temperature, control of environmental disturbances, and selection of measurement methods and measurement devices are some of the factors that need to be considered during the design of the experimental setup. It is also very important that the designed experimental setup must be established with high-quality workmanship. For instance, piping connections and installation of measurement devices must be carried out carefully in a way that does not disturb the flow. The experimental setup must be validated based on the proven known theories before the ultimate experiments. Additionally, calibration of experimental apparatus, logging frequency of the data acquisition system, and measurement of the roughness of test section are some of the points that should be considered during the experiments. References [63, 64], and [65] can help the readers who want to get further information.
- All of the thermophysical and rheological properties of the nanofluids should be measured accurately since these properties are used to calculate the Reynolds number, the Nusselt number and the friction factor. Many researchers determined the thermophysical characteristics of nanofluids using empirical relations that existed in the literature. However, these correlations do not give accurate results. Instead, the thermophysical properties of nanofluids should be measured with calibrated devices after ensuring the stable nanofluid is reached. The stability of the nanofluid should be checked with SEM images and Zeta potential after the preparation of the nanofluid within a time interval. Then, the thermophysical and rheological properties of the nanofluid should be measured with well-calibrated accurate devices.
- The experimental uncertainties should be determined since it is important while interpreting the results. The propagated uncertainty analysis should be conducted for calculated parameters such as heat transfer coefficient, friction factor, the Reynolds number and the Nusselt number. In this context, the method proposed by Cline and McClintock [66] can be used.
- The motion and interaction of the nanoparticles are important in laminar-to-turbulent transition with respect to flow instability. It is reported that flow destabilization was produced by the introduction of nanoparticles, and the smaller the particle size and the higher the particle concentration, the greater the degree of flow instability [67, 68]. Therefore, effective particle size and particle

shape should be measured carefully before the experiments.

- The sedimentation and aggregation are other important parameters. These parameters should be considered and controlled since they dramatically decrease the heat transfer performance of the nanofluids. Additionally, nonuniform distribution of nanoparticles may have an effect on flow instability [68]. Therefore, stability of the nanofluids should be checked with SEM images and Zeta potential after the preparation of the nanofluid within a time interval. This provides a stability time-interval for the corresponding nanofluid and presents its thermal-effective duration.
- For numerical studies, it is essential to tune the coefficients of turbulence model based on the reliable experimental data since most of the turbulence models which detects transition and turbulence-onset are calibrated for external flows.
- The above-mentioned recommendations should be considered in order to draw a solid conclusion on the underlying physical phenomena of laminar-to-turbulent transition of nanofluid flows.

Acknowledgements The first and third authors gratefully acknowledge the financial support of the Istanbul Technical University (ITU) and the Embassy of France in Turkey through the France-ITU Post-doctoral Research Fellowship Program 2019.

References

1. Sahin B. A taguchi approach for determination of optimum design parameters for a heat exchanger having circular-cross sectional pin fins. Heat Mass Transf. 2007;43(5):493. https://doi.org/10.1007/s00231-006-0224-5.
2. Meyer J, McKrell T, Grote K. The influence of multi-walled carbon nanotubes on single-phase heat transfer and pressure drop characteristics in the transitional flow regime of smooth tubes. Int J Heat Mass Transf. 2013;58(1):597–609. https://doi.org/10.1016/j.ijheatmasstransfer.2012.11.074.
3. Sokucu MH, Ozdemir MR. Design and implementation of minichannel evaporator for electronics cooling. J Therm Anal Calorim. 2021;143:3761–73. https://doi.org/10.1007/s10973-020-10457-9.
4. Subasi A. Heat exchanger optimization by response surface method. Master's thesis, Ataturk University, Turkey, 2010.
5. Sheikholeslami M, Gorji-Bandpy M, Ganji DD. Review of heat transfer enhancement methods: focus on passive methods using swirl flow devices. Renew Sustain Energy Rev. 2015;49:444–69. https://doi.org/10.1016/j.rser.2015.04.113.
6. Subasi A, Sahin B, Kaymaz I. Multi-objective optimization of a honeycomb heat sink using response surface method. Int J Heat Mass Transf. 2016;101:295–302. https://doi.org/10.1016/j.ijheatmasstransfer.2016.05.012.
7. Barnoon P, Toghraie D, Dehkordi RB, Abed H. MHD mixed convection and entropy generation in a lid-driven cavity with rotating cylinders filled by a nanofluid using two phase mixture model. J Magn Magn Mater. 2019;483:224–48. https://doi.org/10.1016/j.jmmm.2019.03.108.
8. Moradi A, Toghraie D, Isfahani AHM, Hosseinian A. An experimental study on mwcnt-water nanofluids flow and heat transfer in double-pipe heat exchanger using porous media. J Therm Anal Calorim. 2019;137(5):1797–807. https://doi.org/10.1007/s10973-019-08076-0.
9. Rahimi Gheynani A, Ali Akbari O, Zarringhalam M, Ahmadi Sheikh Shabani G, Alnaqi AA, Goodarzi M, Toghraie D. Investigating the effect of nanoparticles diameter on turbulent flow and heat transfer properties of non-Newtonian carboxymethyl cellulose/CuO fluid in a microtube. Int J Numer Methods Heat Fluid Flow. 2019;29(5):1699–723. https://doi.org/10.1108/HFF-07-2018-0368.
10. Ozdemir MR, Mahmoud MM, Karayiannis TG. Flow boiling of water in a rectangular metallic microchannel. Heat Transf Eng. 2021;42(6):492–516. https://doi.org/10.1080/01457632.2019.1707390.
11. Karayiannis T, Mahmoud M. Flow boiling in microchannels: fundamentals and applications. Appl Therm Eng. 2017;115:1372–97. https://doi.org/10.1016/j.applthermaleng.2016.08.063.
12. Choi SU, Eastman JA. Enhancing thermal conductivity of fluids with nanoparticles. Tech. rep., Argonne National Lab., IL (United States), 1995.
13. Żyła G, Fal J, Estellé P. The influence of ash content on thermophysical properties of ethylene glycol based graphite/diamonds mixture nanofluids. Diam Relat Mater. 2017;74:81–9. https://doi.org/10.1016/j.diamond.2017.02.008.
14. Murshed SS, Estellé P. A state of the art review on viscosity of nanofluids. Renew Sustain Energy Rev. 2017;76:1134–52. https://doi.org/10.1016/j.rser.2017.03.113.
15. Minea AA, Estellé P. Numerical study on CNT nanofluids behavior in laminar pipe flow. J Mol Liq. 2018;271:281–9. https://doi.org/10.1016/j.molliq.2018.08.161.
16. Estellé P, Cabaleiro D, Żyła G, Lugo L, Murshed SS. Current trends in surface tension and wetting behavior of nanofluids. Renew Sustain Energy Rev. 2018;94:931–44. https://doi.org/10.1016/j.rser.2018.07.006.
17. Mahian O, Kolsi L, Amani M, Estellé P, Ahmadi G, Kleinstreuer C, Marshall JS, Siavashi M, Taylor RA, Niazmand H, Wongwises S, Hayat T, Kolanjiyil A, Kasaeian A, Pop I. Recent advances in modeling and simulation of nanofluid flows-part i: fundamentals and theory. Phys Rep, 2019;790:1–48. https://doi.org/10.1016/j.physrep.2018.11.004. https://www.sciencedirect.com/science/article/pii/S0370157318303302. Recent advances in modeling and simulation of nanofluid flows-Part I: Fundamentals and theory.
18. Nikulin A, Moita A, Moreira A, Murshed S, Huminic A, Grosu Y, Faik A, Nieto-Maestre J, Khliyeva O. Effect of Al_2O_3 nanoparticles on laminar, transient and turbulent flow of isopropyl alcohol. Int J Heat Mass Transf. 2019;130:1032–44. https://doi.org/10.1016/j.ijheatmasstransfer.2018.10.114.
19. Wos search. https://apps.webofknowledge.com/ (2021). Accessed 19 Feb 2021
20. Gad-el Hak M. Flow control: passive, active, and reactive flow management. Cambridge: Cambridge University Press; 2000. https://doi.org/10.1017/CBO9780511529535.
21. Subasi A. Numerical and experimental investigation of boundary layer transition with active and passive flow control methods. Ph.D. thesis, Istanbul Technical University, 2017.
22. Sharma K, Sundar LS, Sarma P. Estimation of heat transfer coefficient and friction factor in the transition flow with low volume concentration of al2o3 nanofluid flowing in a circular tube and with twisted tape insert. Int Commun Heat Mass Transf. 2009;36(5):503–7. https://doi.org/10.1016/j.icheatmasstransfer.2009.02.011.

23. Cabaleiro D, Colla L, Agresti F, Lugo L, Fedele L. Transport properties and heat transfer coefficients of ZnO/(ethylene glycol+water) nanofluids. Int J Heat Mass Transf. 2015;89:433–43. https://doi.org/10.1016/j.ijheatmasstransfer.2015.05.067.
24. Saha G, Paul MC. Transition of nanofluids flow in an inclined heated pipe. Int Commun Heat Mass Transf. 2017;82:49–62. https://doi.org/10.1016/j.icheatmasstransfer.2017.02.017.
25. Meyer JP. In: International heat transfer conference digital library (Begel House Inc., 2014).
26. Asirvatham LG, Raja B, Lal DM, Wongwises S. Convective heat transfer of nanofluids with correlations. Particuology. 2011;9(6):626–31. https://doi.org/10.1016/j.partic.2011.03.014.
27. Chandrasekar M, Suresh S, Bose AC. Experimental studies on heat transfer and friction factor characteristics of Al_2O_3/water nanofluid in a circular pipe under transition flow with wire coil inserts. Heat Transf Eng. 2011;32(6):485–96. https://doi.org/10.1080/01457632.2010.506358.
28. Liu D, Yu L. Single-phase thermal transport of nanofluids in a minichannel. J Heat Transfer. 2010;133(3): 031009. https://doi.org/10.1115/1.4002462.
29. Suresh S, Venkitaraj K, Selvakumar P, Chandrasekar M. A comparison of thermal characteristics of Al_2O_3/water and CuO/water nanofluids in transition flow through a straight circular duct fitted with helical screw tape inserts. Exp Therm Fluid Sci. 2012;39:37–44. https://doi.org/10.1016/j.expthermflusci.2012.01.004.
30. Naik M, Janardana GR, Sundar LS. Experimental investigation of heat transfer and friction factor with water-propylene glycol based CuO nanofluid in a tube with twisted tape inserts. Int Commun Heat Mass Transf. 2013;46:13–21. https://doi.org/10.1016/j.icheatmasstransfer.2013.05.007.
31. Zhang J, Diao Y, Zhao Y, Zhang Y. Experimental study of TiO_2 -water nanofluid flow and heat transfer characteristics in a multi-port minichannel flat tube. Int J Heat Mass Transf. 2014;79:628–38. https://doi.org/10.1016/j.ijheatmasstransfer.2014.08.071.
32. Naik MT, Sundar LS. Heat transfer and friction factor with water/propylene glycol-based CuO nanofluid in circular tube with helical inserts under transition flow regime. Heat Transf Eng. 2014;35(1):53–62. https://doi.org/10.1080/01457632.2013.810451.
33. Chougule SS, Sahu S. Heat transfer and friction characteristics of Al_2O_3/water and CNT/water nanofluids in transition flow using helical screw tape inserts - a comparative study. Chem Eng Process Process Intensif. 2015;88:78–88. https://doi.org/10.1016/j.cep.2014.12.005.
34. Selvam C, Irshad EM, Lal DM, Harish S. Convective heat transfer characteristics of water-ethylene glycol mixture with silver nanoparticles. Exp Therm Fluid Sci. 2016;77:188–96. https://doi.org/10.1016/j.expthermflusci.2016.04.021.
35. Xie Y, Zheng L, Zhang D, Xie G. Entropy generation and heat transfer performances of Al_2O_3-water nanofluid transitional flow in rectangular channels with dimples and protrusions. Entropy. 2016. https://doi.org/10.3390/e18040148.
36. Mangrulkar C, Kriplani V, Dhoble A. Experimental investigation of convective heat transfer enhancement using alumina/water and copper oxide/water nanofluids. Therm Sci. 2016;20(5):1681–92. https://doi.org/10.2298/TSCI141225077M.
37. Li Y, Fernández-Seara J, Du K, Álvarez Pardiñas Ángel, Latas LL, Jiang W. Experimental investigation on heat transfer and pressure drop of ZnO/ethylene glycol-water nanofluids in transition flow. Appl Therm Eng. 2016;93:537–48. https://doi.org/10.1016/j.applthermaleng.2015.09.020.
38. Rudyak VY, Minakov AV, Guzey DV, Zhigarev VA, Pryazhnikov MI. On laminar-turbulent transition in nanofluid flows. Thermophys Aeromechanics. 2016;23(5):773–6. https://doi.org/10.1134/S0869864316050164.
39. Zhang J, Diao Y, Zhao Y, Zhang Y. Thermal-hydraulic performance of sic-water and Al_2O_3-water nanofluids in the minichannel. J Heat Transfer. 2015;138(2): 021705. https://doi.org/10.1115/1.4031699.
40. Khairul M, Doroodchi E, Azizian R, Moghtaderi B. The influence of different flow regimes on heat transfer performance and exergy loss of Al_2O_3/di-water and CuO/di-water nanofluids. Appl Therm Eng. 2017;122:566–78. https://doi.org/10.1016/j.applthermaleng.2017.05.035.
41. Osman S, Sharifpur M, Meyer JP. Experimental investigation of convection heat transfer in the transition flow regime of aluminium oxide-water nanofluids in a rectangular channel. Int J Heat Mass Transf. 2019;133:895–902. https://doi.org/10.1016/j.ijheatmasstransfer.2018.12.169.
42. Jamali M, Toghraie D. Investigation of heat transfer characteristics in the developing and the developed flow of nanofluid inside a tube with different entrances in the transition regime. J Therm Anal Calorim. 2020;139(1):685–99. https://doi.org/10.1007/s10973-019-08380-9.
43. Ma J, Xu Y, Li W, Zhao J, Zhang S, Basov S. Experimental investigation into the forced convective heat transfer of aqueous Fe_3O_4 nanofluids under transition region. J Nanoparticles. 2013. https://doi.org/10.1155/2013/601363.
44. Abdul Hamid K, Azmi WH, Mamat R, Usri NA. Advances in materials and manufacturing engineering. Applied mechanics and materials, vol. 660. Wollerau: Trans Tech Publications Ltd; 2014. p. 684–8. https://doi.org/10.4028/www.scientific.net/AMM.660.684.
45. Saha G, Paul MC. Analysis of heat transfer and entropy generation of tio2-water nanofluid flow in a pipe under transition. Procedia Eng. 2015;105:381–7. https://doi.org/10.1016/j.proeng.2015.05.023. http://www.sciencedirect.com/science/article/pii/S1877705815008206. The 6th BSME International Conference on Thermal Engineering.
46. Amiri A, Ahmadi G, Shanbedi M, Etemadi M, Mohd Zubir MN, Chew BT, Kazi SN. Heat transfer enhancement of water-based highly crumpled few-layer graphene nanofluids. RSC Adv. 2016;6:105,508-105,527. https://doi.org/10.1039/C6RA22365F.
47. Kudratillayevich ST, Ugli IAA. Measurement of coefficient of convective heat transfer based on silicon oxide nanofluid in the cylindrical channel. Eur Sci Rev. 2017;3–4:102–4.
48. Logesh K, Arulprakasajothi M, Renish RR, Venkatasudhahar M, Raja ND. Impact of water-based tio2 nanofluid on heat transfer under transition flow. Mater Today Proc. 2018;5(9, Part 3):20,544 – 20,548. https://doi.org/10.1016/j.matpr.2018.06.432. http://www.sciencedirect.com/science/article/pii/S2214785318315621. Materials Processing and characterization, 16th – 18th March 2018.
49. Steele A, Bayer I, Allen K, Loth E. Effect of carbon nanotube additives on drag reduction in pipe flows. 2009. https://doi.org/10.1115/FEDSM2009-78122.
50. Singh PK, Sundararajan T, Das SK. Hydrodynamic study of nanofluids in microchannel. 2009. https://doi.org/10.1115/MNHMT2009-18180.
51. Goutam S, Paul MC. Discrete phase approach for nanofluids flow in pipe. 2014. https://doi.org/10.15224/978-1-63248-054-5-59. http://eprints.gla.ac.uk/99996/.
52. Demirkır Çayan, Ertürk H. Convective heat transfer and pressure drop characteristics of graphene-water nanofluids in transitional flow. Int Commun Heat Mass Transf. 2021;121:105,092. https://doi.org/10.1016/j.icheatmasstransfer.2020.105092.
53. Briclot A, Henry J, Popa C, Nguyen C, Fohanno S. Experimental investigation of the heat and fluid flow of an Al_2O_3-water nanofluid in the laminar-turbulent transition region. Int J Therm Sci. 2020;158:106,546. https://doi.org/10.1016/j.ijthermalsci.2020.106546.

54. Al-Zuhairy RC, Kareem ZS, Abdulhadi AA. Al_2 O_3-water nanofluid heat transfer enhancement of a twin impingement jet. Case Stud Therm Eng. 2020;19:100,626. https://doi.org/10.1016/j.csite.2020.100626.
55. Duangthongsuk W, Wongwises S. An experimental study on the heat transfer performance and pressure drop of TiO_2-water nanofluids flowing under a turbulent flow regime. Int J Heat Mass Transf. 2010;53(1):334–44. https://doi.org/10.1016/j.ijheatmasstransfer.2009.09.024.
56. Olivier JA, Meyer JP. Single-phase heat transfer and pressure drop of the cooling of water inside smooth tubes for transitional flow with different inlet geometries (rp-1280). HVAC R Res. 2010;16(4):471–96. https://doi.org/10.1080/10789669.2010.10390916.
57. Meyer J, Olivier J. Transitional flow inside enhanced tubes for fully developed and developing flow with different types of inlet disturbances: Part I—adiabatic pressure drops. Int J Heat Mass Transf. 2011;54(7):1587–97. https://doi.org/10.1016/j.ijheatmasstransfer.2010.11.027.
58. Meyer J, Olivier J. Transitional flow inside enhanced tubes for fully developed and developing flow with different types of inlet disturbances: Part II-heat transfer. Int J Heat Mass Transf. 2011;54(7):1598–607. https://doi.org/10.1016/j.ijheatmasstransfer.2010.11.026.
59. Shah R, London A. laminar flow forced convection in ducts: a source book for compact heat exchanger analytical data. Advances in geophysics. Academic Press, 1978. https://books.google.com.tr/books?id=FtNFAQAAIAAJ.
60. Gnielinski V. New equations for heat and mass transfer in the turbulent flow in pipes and channels. NASA STI/Recon Tech Rep A. 1975;41(1):8–16.
61. Xuan Y, Li Q. Investigation on convective heat transfer and flow features of nanofluids. J Heat Transf. 2003;125(1):151–5.
62. Dittus F, Boelter L. Heat transfer in automobile radiators of the tubular type. Int Commun Heat Mass Transf. 1985;12(1):3–22. https://doi.org/10.1016/0735-1933(85)90003-X.
63. Mills C. Identifying the transition between laminar and turbulent flow using high-frequency pressure loss measurement. Ph.D. thesis, Coventry University. 2020.
64. Bashir AI, Everts M, Meyer JP. Influence of inlet contraction ratios on the heat transfer and pressure drop characteristics of single-phase flow in smooth circular tubes in the transitional flow regime. Exp Therm Fluid Sci. 2019;109:109,892.
65. Everts M, Meyer J. Heat transfer of developing and fully developed flow in smooth horizontal tubes in the transitional flow regime. Int J Heat Mass Transf. 2018;117:1331–51. https://doi.org/10.1016/j.ijheatmasstransfer.2017.10.071.
66. Kline SJ, McClintock FA. Describing uncertainties in single-sample experiments. Mech Eng. 1953;75(1):3–8.
67. Rudyak VY, Bord EG. On stability of plane and cylindrical poiseuille flows of nanofluids. J Appl Mech Tech Phys. 2017;58(6):1013–20. https://doi.org/10.1134/S0021894417060074.
68. Lin J, Yang H. A review on the flow instability of nanofluids. Appl Math Mech. 2019;40(9):1227–38. https://doi.org/10.1007/s10483-019-2521-9.